Chapter 7

GEOLOGY OF THE BASE METAL SULFIDE ZONES AND ALTERATION HALO OF THE ONEDIN PROSPECT

7.1 INTRODUCTION

The prospects at Koongie Park have been considered to be VHMS-type deposits since they were discovered in the 1960s. Kennecott Exploration (Australia) Ltd. and Asarco Australia Ltd. geologists drilling at Sandiego suggested that the relationship between the sulfide mineral zone, hosted in an interval of possible hydrothermal chert and ironstone ('Mimosa member'), overlying a pyroclastic substrate ('Coolibah tuff') and capped by lava ('Weldons lava'), is consistent with typical VHMS deposits. They envisaged the deposits as vent representing former sites on the ocean floor, which were subsequently buried by lava flows (Sewell, 1999). Although not documented, alternative genetic models for these deposits, debated by exploration geologists include: (1) distal skarn deposit[1]; and (2) structurally controlled replacement-type deposits, formed during deformation within high strain zones, e.g., Rosebery (Aerden 1990, 1991, 1993).

Two types of base metal occurrences, associated with different alteration halos in the KPF at Koongie Park, are:

1. Low-grade massive sulfide deposits at Hanging Tree and Puseye related to surficial ironstones, albite+ quartz alteration facies in the hanging wall and talc+tremolite alteration facies in the footwall.
2. Larger deposits at Sandiego, Onedin and the base metal occurrences at Onedin South, Gosford and Rockhole (Table 2.3) hosted by chloritic mudstone and carbonate, with chloritic footwall facies and chlorite+talc+carbonate + quartz alteration facies overprinting albite + quartz alteration facies in the hanging wall.

Preservation of sulfide minerals in drillcore, access to footwall exposure and interest in the carbonate-host sulfide zones at Onedin focussed attention on this prospect.

This chapter of the thesis examines the alteration halo and base metal sulfide occurrences at Onedin. It commences with a review of the geology at Onedin and description of the morphology of the sulfide zones. Following this review, is a discussion of the effects of deformation and metamorphism on the sulfide zones, highlighting features in sulfide minerals. The effects of alteration and the base metal mineralisation are examined and their relationships explored. This information is compared to skarn and structural origins for the sulfide deposits. The sulfide zones are best interpreted as sub-seafloor VHMS deposits, which have been overprinted by later deformation and metamorphism. Modern and a few well documented ancient examples of sub-seafloor VHMS deposits are reviewed and compared to Onedin. The mineral assemblage is used to

[1] A skarn deposit is defind as 'sulfide and gangue minerals deposited as a result of contact metamorphism and pneumarolytic metasomatism of carbonate or carbonate-bearing rock' (Lentz 1998b).

constrain sulfide forming conditions and is instrumental in developing a genetic model for the formation of the base metal occurrences at Onedin, which is presented in the last section of the chapter.

7.2 THE ONEDIN BASE METAL PROSPECT

7.2.1 GEOLOGY OF THE ONEDIN PROSPECT

The Onedin prospect lies on the southeastern limb of a large F_{KP2} antiform (1:25 000 map, backpocket). The Onedin Member, comprised of ironstone, black mudstone and turbiditic sandstone and mudstone (Chapters 2, 4) hosts the mineralised zone. A quartz-bearing mudstone sequence forms the footwall and the hanging wall is dominated by an aphyric rhyolitic sill with minor sandstone and mudstone. Late basalt dykes cross across the sequence (Chapter 4, Fig. 7.1). The contact between footwall and the host sequence is faulted. The contact between the hanging wall and the Onedin Member is both discordant and concordant, and in places peperitic (Chapters 4, 5).

The Onedin Member at Onedin is folded by F_{KP1} folds and refolded by F_{KP2} structures plunging at 60° to the southwest. Steep northeast to ENE faults cut the folds to form a faulted f lower structure (Fig. 7.1). This interpretation of the structure at Onedin is different to the simpler interpretation of an F_{KP2} synform-antiform couplet by Sewell (1999) (Fig. 7.1B). The influence of the F_{KP1} fold was considered significant as small F_{KP1} folds are apparent at outcrop scale (Chapter 3) and appear to control the shape of the gossan (Ransom 1990). The faults display displacements of up to 60 m. In core, faults are recognised as fracture zones associated with low level base metal grades, limonitic and clay minerals well below the weathering limit, or thick blocky quartz veins.

Although this model explains many of the units and features intersected in the main drillholes at the prospect, and is consistent with the structural overprinting in this domain, some problems are unresolved. One problem is the greater thickness of the Onedin Member above the F_{KP1} fold (100 m thick) compared to beneath it (50 m thick). Possible explanations are faulting, lateral facies changes and thickening of the Onedin Member, or discordant contacts between the Onedin Member and the rhyolitic sill. A fault bounded block of intensely altered, footwall quartz-bearing mudstone, intersected at the end of KPD 32 (401–415 m), is also anomalous. It is not shown in the cross-section in Figure 7.1D and is also missing from the cross-sectional model of Sewell (1999).

In the northern part of the prospect, and at depth, the host sequence is 40–50 m thick. Near the surface at Onedin it appears to be 100–150-m thick. Folding alone cannot account for this, so the Onedin Member must thickens in this area (Chapter 4). Next to the host sequence, the footwall displays semi-conformable zones composed of quartz + chlorite + white mica with quartz + chlorite + pyrite and quartz + talc near the contact. Quartz + chlorite + talc and chlorite + talc + carbonate ± actinolite/tremolite are the main gangue minerals. The hanging wall rhyolite contains quartz + albite overprinted by chlorite + white mica.

Disseminated sulfide minerals, generally pyrite, exist in the upper parts of the footwall associated with quartz and chlorite. Disseminated pyrite, pyrrhotite and minor chalcopyrite are scattered throughout the sedimentary units of the Onedin Member. Magnetite is abundant in

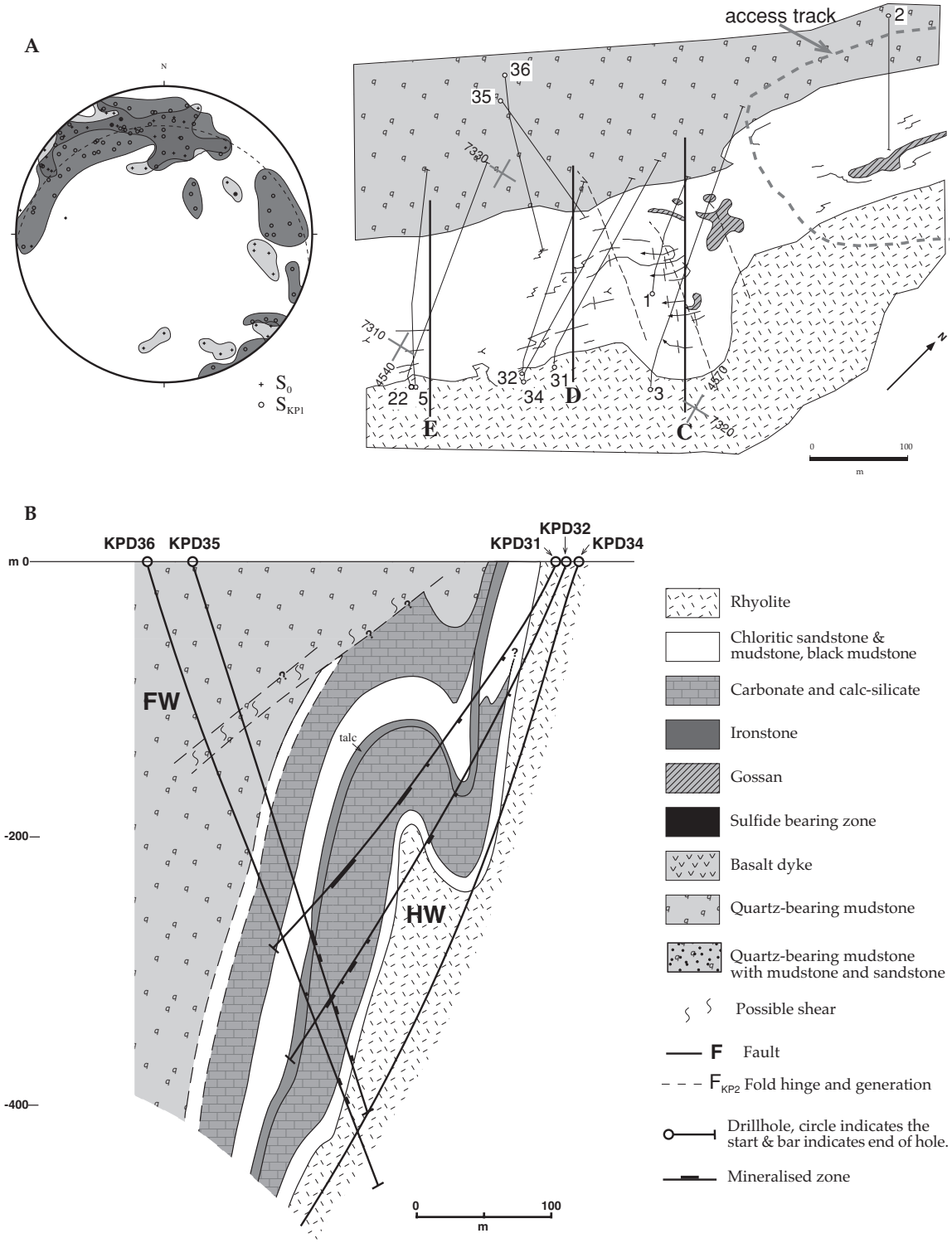

Figure 7.1 Map and cross-sections of the geology at Onedin. (A) Map of the prospect with stereonet plot of bedding and early cleavages. Gossan and folds are outlined and cross-sections C, D, and E located. The plunge of the second generation folds (FKP2) is around 60_i, steeper in the northeast and shallowing to the southwest. (B) Onedin geology model proposed by Sewell (1999). C, D, and E (following pages) are cross-sections from Onedin, looking north.

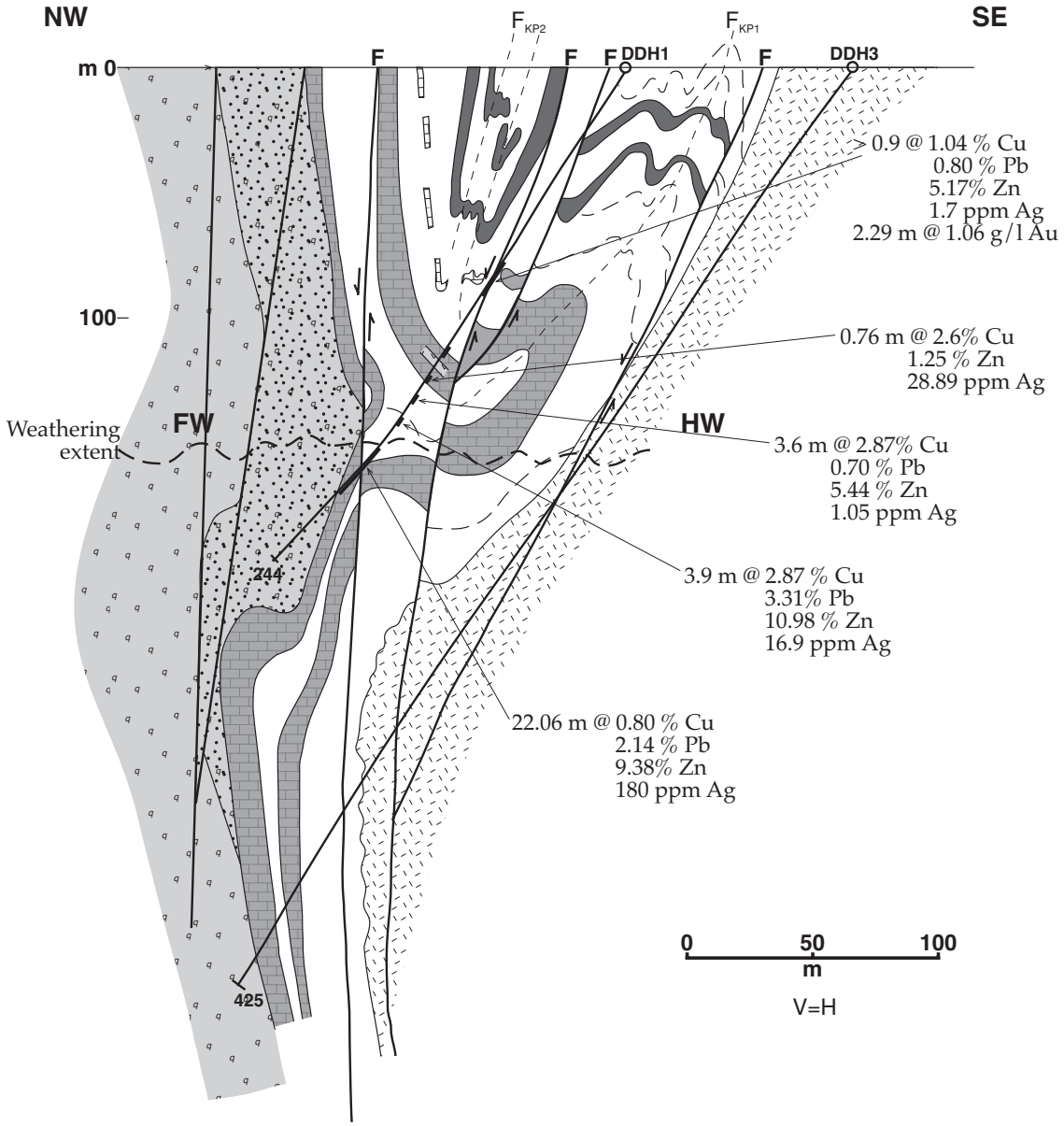

Figure 7.1 (C) Section through the northern portion of Onedin incorporating DDH 1 and DDH 3, looking north. For legend see Figure 7.1B.

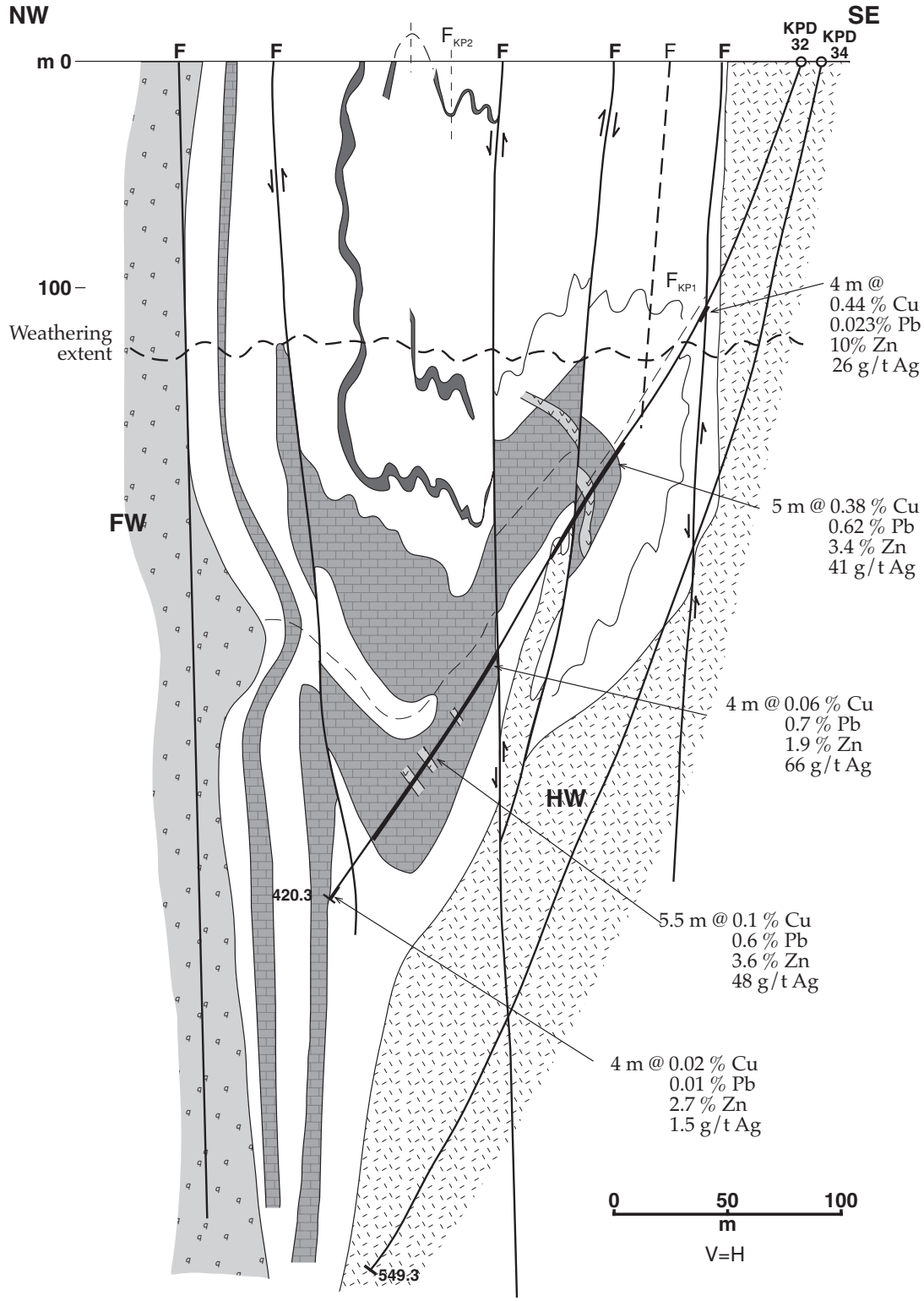

Figure 7.1 (D) Section through the central part of Onedin prospect, incorporating KPD 32 and 34, looking north. For legend see Figure 7.1B.

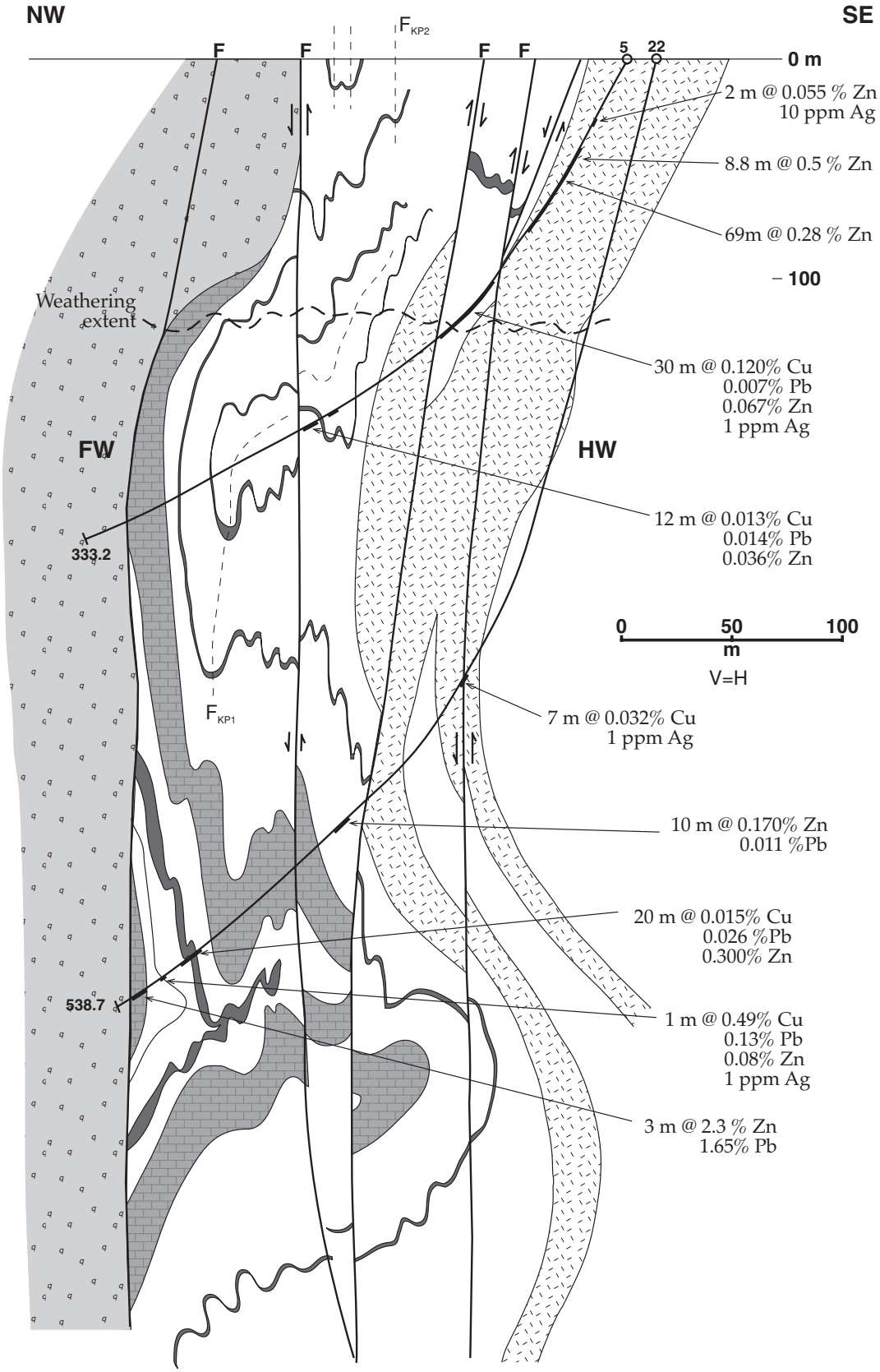

Figure 7.1 (E) Southern section through the southern part of Onedin, incorporating DDH 5 and 22, looking north. For legend see Figure 7.1B.

ironstone and is disseminated in many chlorite- and quartz-bearing sedimentary rocks. Magnetite is associated with sulfide minerals in the upper parts of the upper carbonate lens at the northern end of the prospect, in the middle and lower portions of the upper carbonate lens in the central part of the prospect, and disseminated above the upper carbonate lens and into the rhyolitic sill in the deeper parts of the prospect. In all cases, the magnetite appears to pre-date the sulfide minerals. Some magnetite has a needle-like morphology and may be replacing precursor haematite or early-formed pyrrhotite. Discontinuous(?), and stratabound base metal sulfide zones are hosted by carbonate and quartz-chlorite schist.

7.2.2 BASE METAL SULFIDE ZONES

Patches and lenses of sulfide minerals have been intersected along a 600 m strike length at Onedin, but are concentrated in a series of southwest plunging folds, south of the access track (Fig. 7.1). A subdued gossan is formed by the interference of F_{KP1} and F_{KP2} folds and marks a carbonate-hosted sulfide lens at the surface (GR 4563 7334). The gossan is massive brown-black goethite, with some radiating, translucent malachite encrustations and stringers of chrysocolla and malachite. Sulfide boxworks are abundant (Warne et al. 1976).

Nine drillholes constrain the massive sulfide bodies subsurface. Massive sulfide intervals are thickest, and metal grades highest, in the northern and central parts of the prospect. The overall grade (1Mt @11%Zn, 1% Pb and 1% Cu, Sewell 1999), indicates that Zn is the most abundant metal. It is accommodated by sphalerite. Less abundant Cu and Pb are in chalcopyrite and galena respectively. Triplots of Zn, Cu and Pb, illustrate that the sulfide zones at Onedin are generally of Zn-Cu or Zn-Pb-Cu types (Solomon 1976, Huston & Large 1987, Large 1992) (Fig. 7.2). Silver abundance is variable, with small grains of Ag-bearing sulfosalts, probably freibergite (Cu, Zn, Fe,

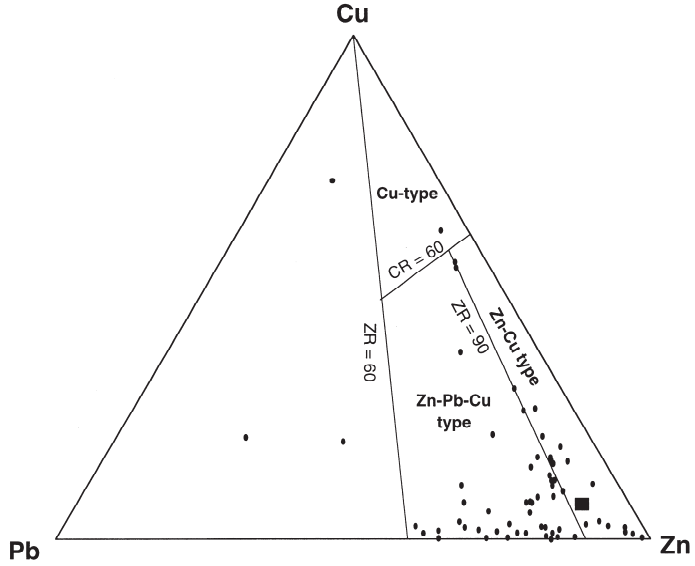

Figure 7.2 Triplot of Cu-Pb-Zn for the massive sulfide intervals at Onedin. The square represents the overall mean grade (Sewell 1999). Fields of different sulfide zones are Cu-type for Cu ratio above 60 (Cu ratio = 100 Cu/Cu+Zn), Zn-Pb-Cu types for those with Zn ratios between 60 and 90 (Zn ratio = 100 Zn/ Zn + Pb) and Zn-Cu type, where the Zn ratio is greater than 90 (Solomon 1976, Huston & Large 1987, Large 1992). Most of the sulfide zones at Onedin classify as either Zn-Pb-Cu type or Zn-Cu type and the overall base metal grade plots as a Zn-Cu type. Only one near-surface sample in DDH 1 has a Zn ratios less than 60 and only one sample from the southern end of the deposit has a Cu ratio greater than 60. The latter may be due to overall low grades in this part of the prospect.

Figure 7.3 Photographs of core from the base metal sulfide zones at Onedin:
(A) Carbonate-hosted massive sulfide with abundant sphalerite surrounding "pseudofragments" (arrowed) of veined and altered carbonate+talc+chlorite. The bottom sample exhibits layering of sphalerite, chlorite, talc and carbonate minerals.
(B) Chlorite schist-hosted sulfide from KPD 35. Pyrite is abundant in these samples which display layered, massive and veined textures. Other sulfide minerals include pyrrhotite, chalcopyrite, galena and sphalerite. The gangue consists of dark chlorite, chlorite and quartz, carbonate, associated with sphalerite (e.g., light area in 334.3 m) and quartz veins and veinlets.
(C) Quartz+chalcopyrite veins criss-cross siliceous sedimentary rocks in core between KPD 32 183–186 m. These veins are cut by chlorite+carbonate+sphalerite+chalcopyrite veins (arrowed).

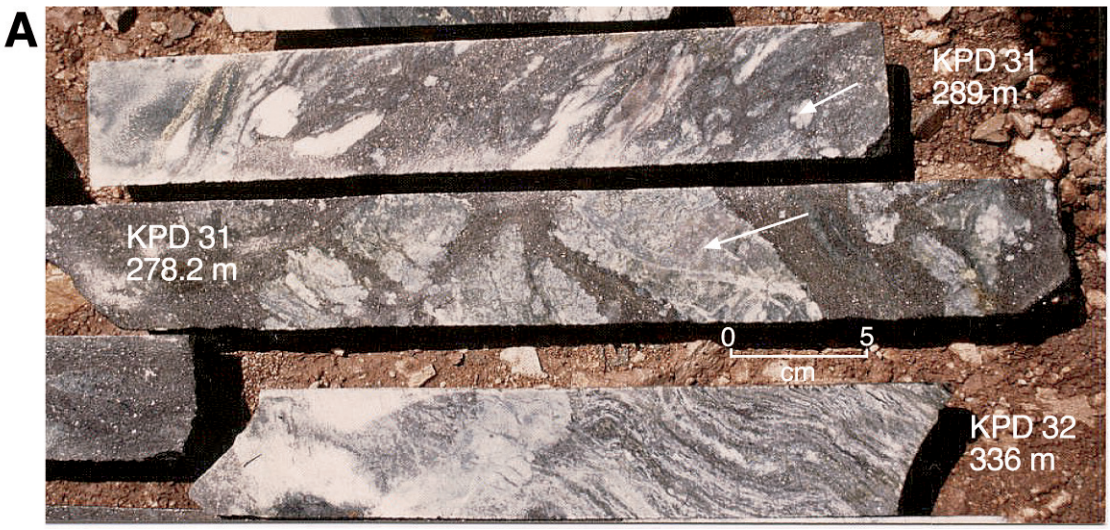
A
KPD 31
289 m
KPD 31
278.2 m
0
5
cm
KPD 32
336 m

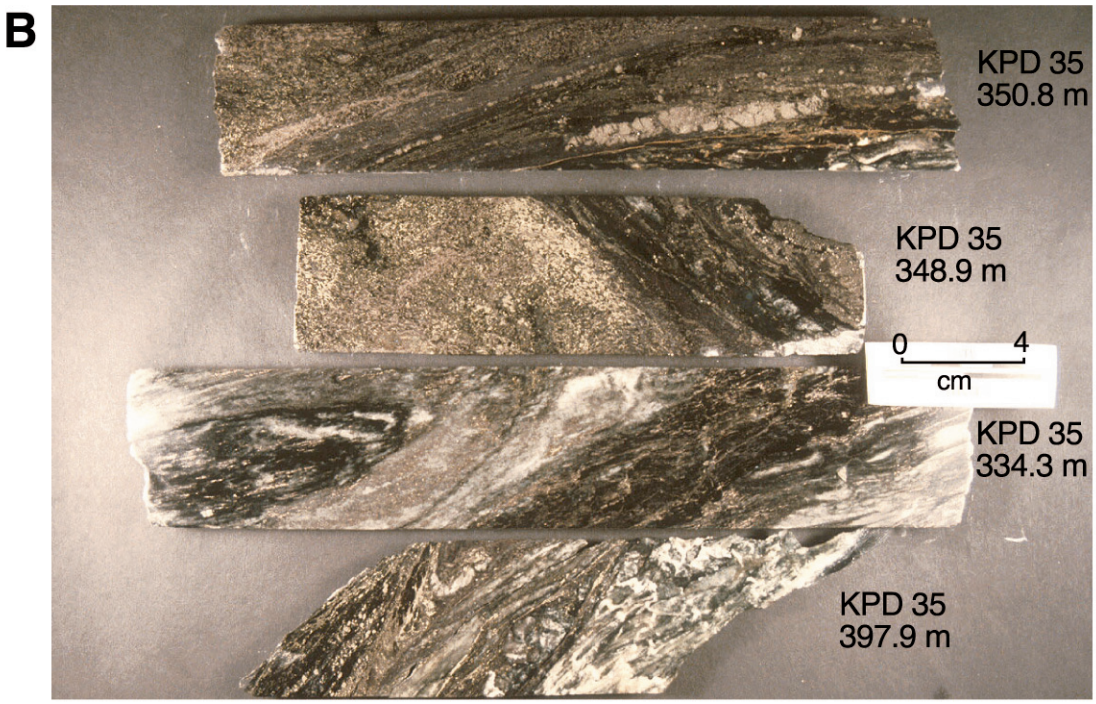
B
KPD 35
350.8 m
KPD 35
348.9 m
0
4
cm
KPD 35
334.3 m
KPD 35
397.9 m

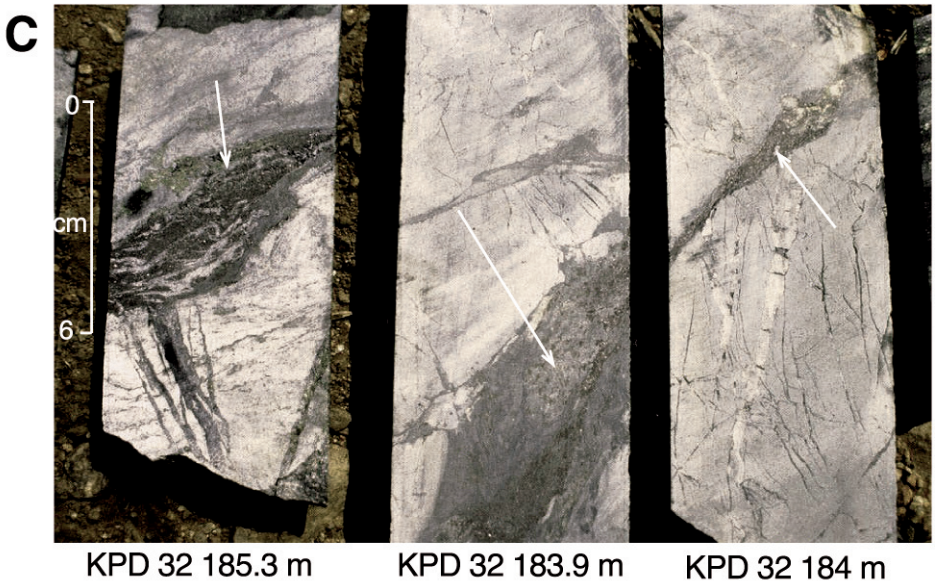
C
0
cm
6
KPD 32 185.3 m
KPD 32 183.9 m
KPD 32 184 m

$Ag)_8Sb_2S_7$ in high Ag samples such as KPD 31 210 m (323 g/t Ag). Au is significant only in one interval, from the weathered and oxidised zone (DDH 1 115–118 m 1.06 g/t Au) (Woodhouse 1989, Sewell 1999), which may be related to a fault. The refolding model for the units hosting the sulfide zone at Onedin, will not greatly impact on the informal reserve estimates of Sewell (1999) (see above).

Carbonate-hosted sulfide zones

Two carbonate lenses are present. Both lenses contain sulfide minerals, but the upper lens forms the host for most of the massive sulfide intersected in the northern and central parts of the prospect. The lower carbonate lens, intersected in KPD 35 and KPD 36, contains disseminated sulfide minerals. Elsewhere, the lower carbonate has not been fully tested. Both carbonate lenses are at least 10 m thick, although the upper lens thickens up to 60 m thick in the hinge of the F_{KP1} fold (Fig 7.1D).

In carbonate-hosted sulfide zones, sphalerite is the most abundant sulfide mineral. Sphalerite is associated with less abundant chalcopyrite and pyrrhotite and minor pyrite and galena. Massive fine to coarse (0.1–1 mm across) recrystallised, red to orange sphalerite grades into sphalerite-dominated pseudobreccias (Fig. 7.3A). Ragged-edged 'fragments' of dolomite or fine-grained (0.02 mm) quartz, form an open framework in a matrix of sphalerite, dolomite or calcite. Some pseudoclasts are complexely veined by carbonate. Gangue minerals include dolomite, ferroan dolomite, ankerite (Chapter 8), talc and less abundant chlorite and quartz (Fig.7.3A).

Replacement textures of sulfide minerals are abundant in the carbonate-hosted sulfide zones (Fig. 7.4A). Sphalerite grew on the edges of large carbonate crystals (0.5 mm) in association with small (0.05–0.1 mm), Fe-rich dolomite crystals and chlorite. Most sulfide mineral textures are annealed in the carbonate-hosted sulfide zones. Sphalerite often encloses irregularly shaped crystals of chalcopyrite, pyrrhotite, pyrite and minor galena (Fig. 7.4B). Pyrrhotite is the dominant iron sulfide mineral, with some spongy and cubic pyrite (Fig. 7.4C). Pyrite is most abundant on the outer edges of the carbonate-hosted sulfide zones. In the deeper sections of the upper carbonate lens, pyrite displays radiating and replacement textures (Fig 7.4D). Accessory bismuthanite, and freibergite occur as small (<0.5 mm across), irregular shaped crystals in the massive sulfide, surrounded by sphalerite and associated with pyrrhotite.

Chlorite schist-hosted sulfide zones

In the deeper sections of the prospect, veins of pyrrhotite, pyrite and chalcopyrite are present in chlorite schist between the carbonate lenses (Fig. 7.1). Two chlorite schist-hosted sulfide intervals were intersected above the upper carbonate lens in the central portion of the prospect. Sulfide minerals are continuous from the top of the upper carbonate lens into overlying chlorite schist in KPD 31 and 32 (Fig. 7.5). Chlorite schist-hosted sulfides occur in the northern part of the prospect between the carbonate lenses in DDH 1 (Fig. 7.1). In the southern portion of the prospect, where grades are lower, chlorite schist-hosted sulfide occur above the upper carbonate lens in DDH 5 (120–150 m, 245–259 m) and deeper in DDH 22 (390–395 m), and between the two carbonate lenses (DDH 22 470–480 m, Fig. 7.1).

Pyrite, sphalerite, chalcopyrite and minor pyrrhotite and galena in these zones are associated with carbonate, chlorite, talc and quartz. In some veins, chalcopyrite or pyrrhotite are the only

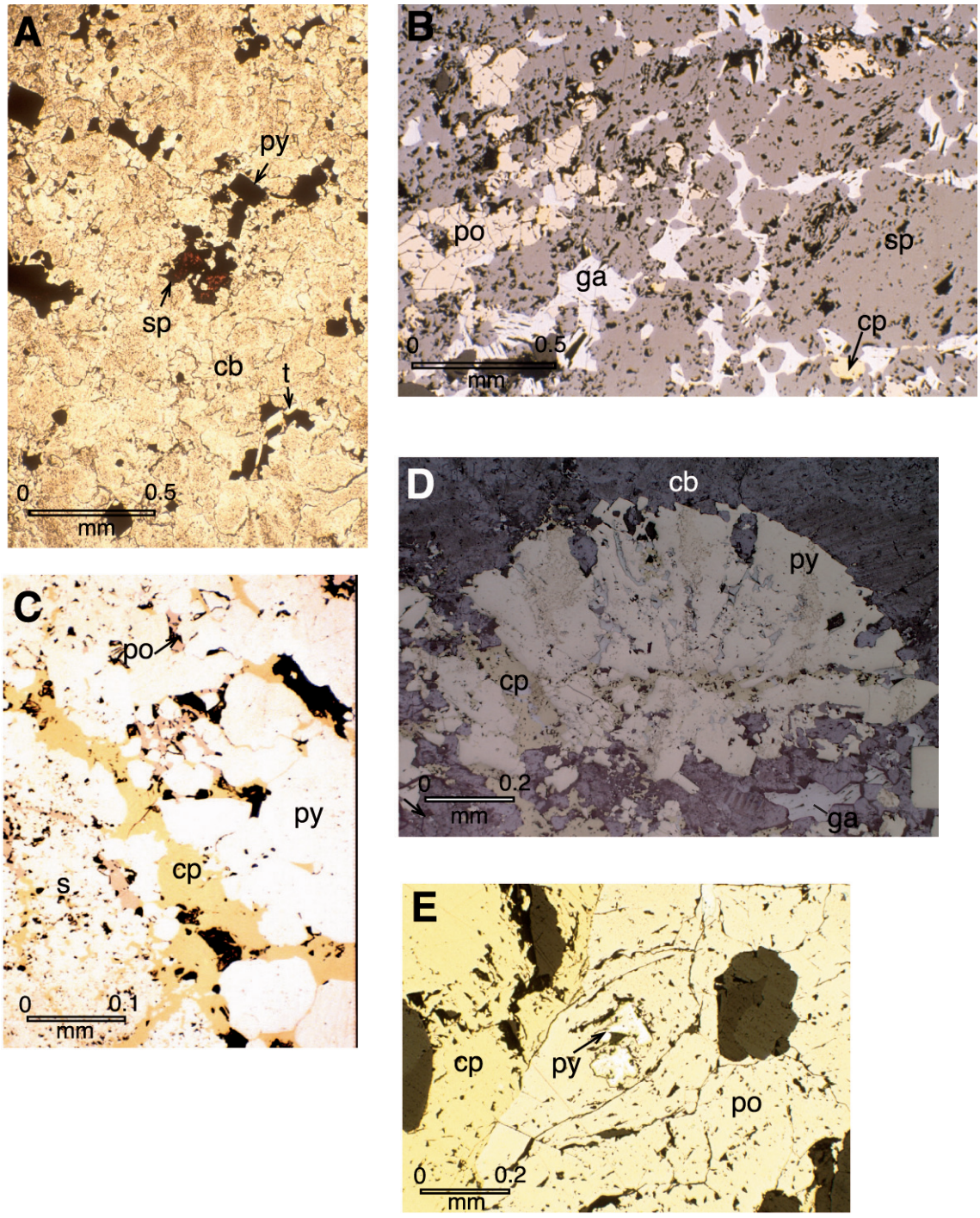

Figure 7.4 Photomicrographs of some sulfide minerals from Onedin: (A) Disseminated sphalerite (sp) and pyrite (py) replace carbonate (cb) along grain boundaries. Some talc (t) grown with the pyrite (KPD 31 315.5 m, x 50, ppl). (B) Annealed textures typical of most of the massive sulfide. Sphalerite (sp) encloses irregularly shaped galena (ga), pyrrhotite (po) and minor chalcopyrite (cp, KPD 32 336.2 m, x 50, reflected-light). (C) Spongy pyrite (s) and cubic pyrite (py) with minor pyrrhotite (po) and interstitial chalcopyrite (cp, KPD 32 329 m, x 200, reflected-light). (D) Radiating pyrite (py) with outer cubic pyrite from the top of the upper carbonate lens. Spaces are infilled with chalcopyrite (cp). Minor galena (ga) is present in the carbonate (cb) gangue (KPD 35 383 m, x 100, reflected-light). (E) Pyrite cube (py) within pyrrhotite (po, KPD 32 320 m, x 100, reflected-light).

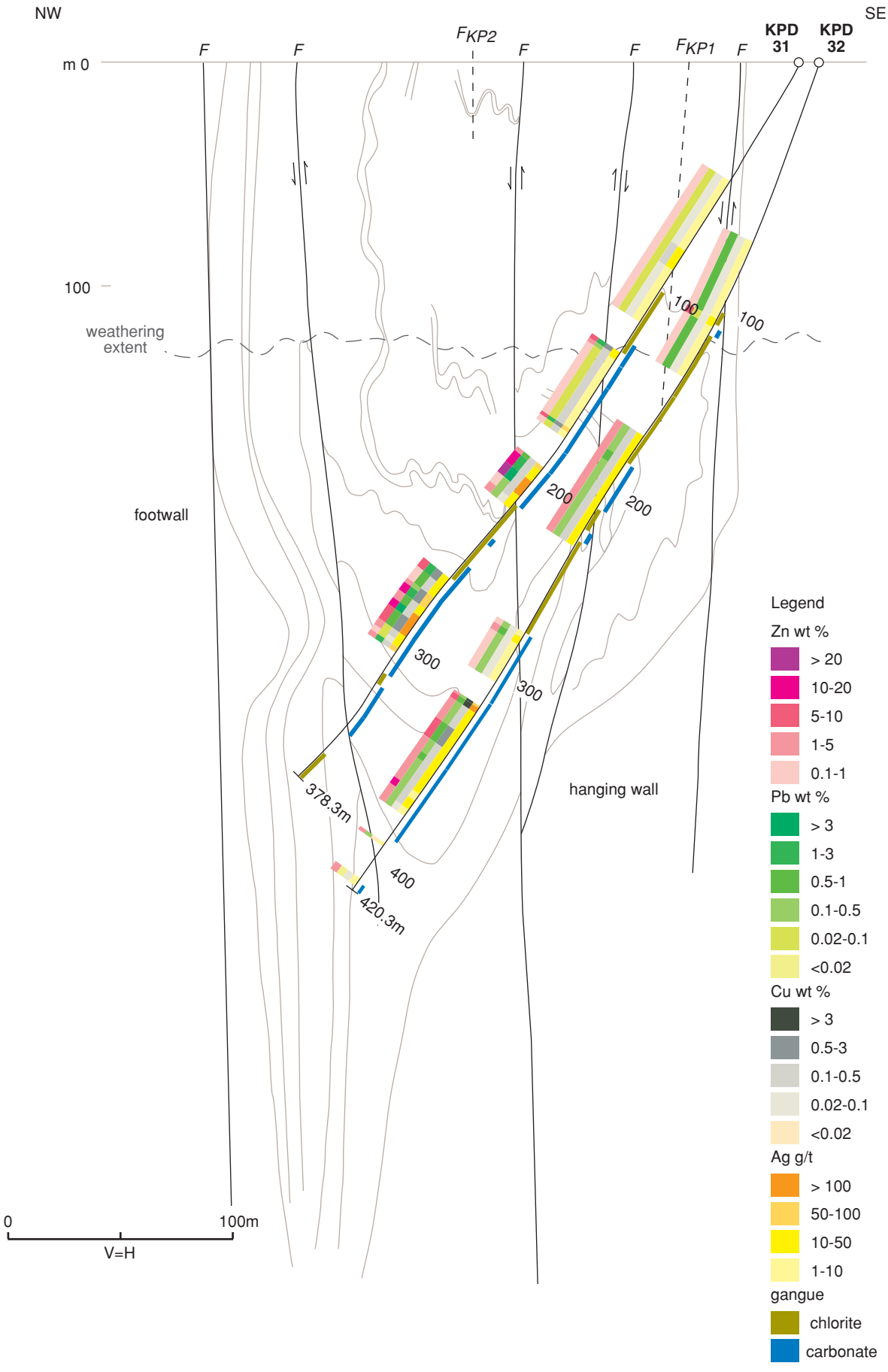

Figure 7.5 Downhole assay results for Zn, Pb, Cu (in wt%) and Ag (in g/t) for KPD 31 and 32 in the central portion of the Onedin prospect. Major gangue mineral is represented on the lower side of the drillholes. The highest grades are coincident with carbonate.

sulfide minerals. Where there was a pre-existing silicification, sulfide minerals were restricted to veins. An example is from the silicified top of the upper carbonate lens in KPD 32 188m, where the host is cross-cut by quartz+chalcopyrite veins (<5 cm across, Fig. 7.3C). Layering of gangue and sulfide minerals is evident in some parts of the chlorite schist-hosted sulfide zones. It may be where mineralising fluids followed bedding or be produced, or enhanced, by deformation (Fig. 7.3B).

7.2.3 DESCRIPTIONS AND MINERAL CHEMISTRY OF THE SULFIDE MINERALS AT ONEDIN

The most abundant sulfide mineral in the sulfide zones at Onedin is sphalerite. Pyrrhotite and pyrite are also abundant along with chalcopyrite. Galena is less abundant. Minor freibergite is present in high silver zones. Each of these minerals is described and microprobe data on trace elements within the minerals presented where completed. The minerals are discussed in order of abundance.

Sphalerite

Coarse (<2 mm) red, iron-rich (10–13 mol% FeS) sphalerite is the most abundant mineral in the carbonate-hosted massive sulfide lenses. Iron content of the sphalerite in the chlorite schist-hosted ore is at the lower end of this range (av. 10 mol% FeS). Doubly polished thin-sections reveal no internal zonation or variation (Figs 7.6A, 7.7A), although some microprobe analyses show fluctuations in Fe content (Appendix 4). Massive sphalerite patches with interstitial galena are interspersed with pyrrhotite, chalcopyrite and minor pyrite.

Most sphalerite analysed is from the carbonate-hosted lenses in the central part of the Onedin prospect (Table 7.1). Sphalerite can contain up to 0.31 wt% Cd. Co is elevated (0.19-0.25 mol% CoS) in one sample, coincident with elevated Cu and Cd (KPD 32 336 m). Only traces of Mn occur in the sphalerite (Mn 0.02-0.09 wt%). Sn is absent from the sphalerite analysed and Ga, In or Hg are rarely above detection limits (Table 7.1, Appendix 4).

Pyrrhotite

Pyrrhotite is the main iron sulfide mineral formed during mineralisation at Onedin. It is abundant in the carbonate hosted sulfide zones. It is less abundant in parts of the chlorite schist-hosted sulfide zones, especially in veins dominated by chlorite and carbonate. Evidence of deformation-related pyrrhotite is in veins which cross-cutting ironstone and late piercement veins.

No trace element data was gathered on this mineral.

Pyrite

Pyrite occurs in all the sulfide zones and grew during sulfide mineralisation and deformation. Early pyrite, pseudomorphing blade-like crystals, and radiating pyrite (Fig. 7.4D) formed during the main mineralising event. Late metamorphic pyrite have grown in pyrrhotite (Fig. 7.4E), exhibit a cubic habit and can overprint all foliations (Fig. 7.6B).

Pyrite was analysed for minor elements in samples from the carbonate-hosted massive sulfide lenses, in the central portion of the prospect. One specimen is from a chlorite schist-hosted sulfide zone (KPD 32 120.7 m). The results indicate that Co is present in significant amounts (1.25 wt%) in pyrite in deeper parts of the upper carbonate-lens and that pyrite in the upper carbonate lens can

Figure 7.6 Structural and metamorphic overprinting features of the altered and mineralised rocks at Onedin.
(A) Deformed gangue minerals, including talc (t) and chlorite (ch), distorted by solid state flow of the surrounding red sphalerite (sp) and pyrrhotite (po) during remobilisation (KPD 32 366.2 m, x 50, ppl).
(B) Photomicrograph of late idioblastic pyrite cross-cutting foliation defined by the alignment of talc flakes (t) amongst sphalerite (sp) and carbonate (cb, KPD 32 350 m, x 25, ppl).
(C) Late vein of chalcopyrite (cp), galena and carbonate (cb) cross-cutting a fold (F_{KP2}) in chlorite-rich rock (ch). S_{KP1} foliation, defined by aligned chlorite, is folded (KPD 31 289 m, x 12.5, ppl).
(D) Layers of sulfide and gangue minerals, mainly pyrrhotite (po) with chlorite, galena (ga) and a layer containing cubic pyrite (py), which has experienced brittle deformation (KPD 35 350 m).
(E) Core from KPD 31 177.8 showing folded, thinly interbedded, chloritic sandstone and mudstone with a well developed foliation. The foliation is in part defined by patches of pyrite and pyrrhotite (arrow).
(F) Pyrrhotite, pyrite and sphalerite, between layers of talc, carbonate and quartz that has been folded around FKP2 (KPD 32 187 m).
(G) Photomicrograph of a piercement vein cross-cutting carbonate (cb) and chlorite (ch) with minor pyrite (py). The vein is filled by quartz (q) with the forked termination infilled by pyrite (KPD 32 300.2 m, x12.5, ppl).

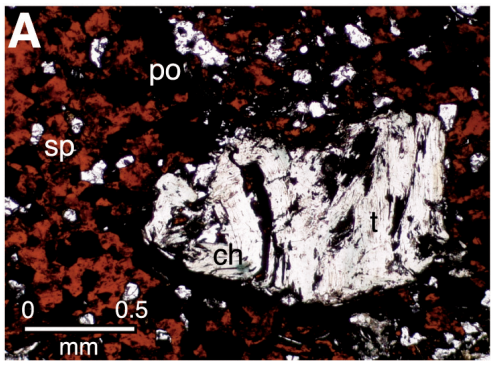
A
po
sp
t
ch
0
0.5
mm

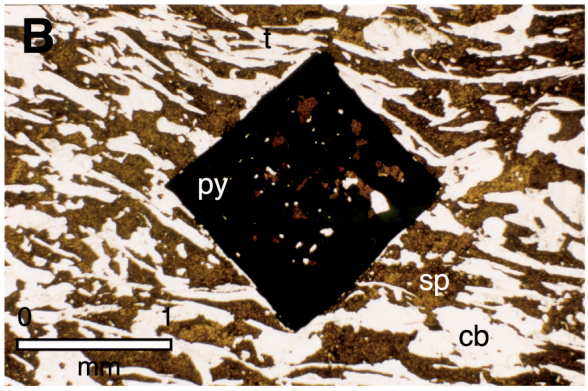
B
t
py
sp
cb
0
1
mm

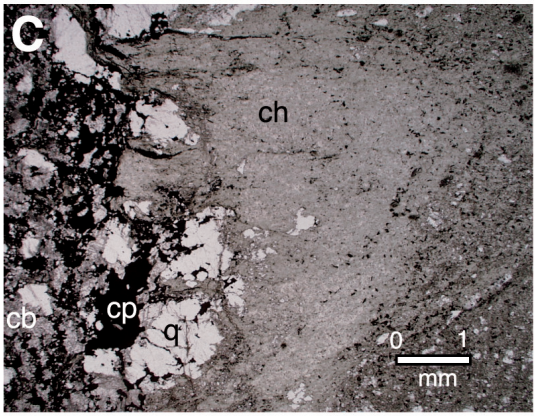
C
ch
cb
cp
q
0
1
mm

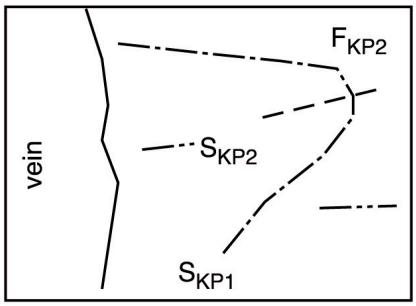
vein
F_{KP2}
S_{KP2}
S_{KP1}

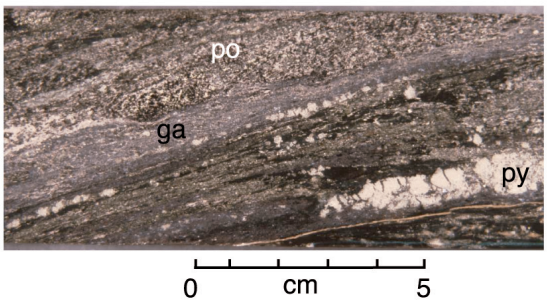
D
po
ga
py
0
cm
5


F
0
cm
5

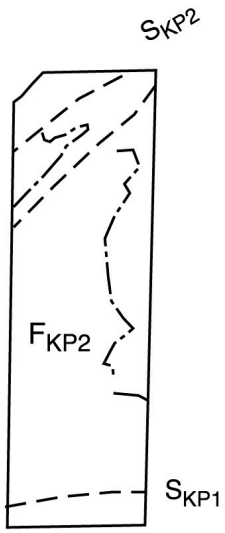
S_{KP2}
F_{KP2}
S_{KP1}

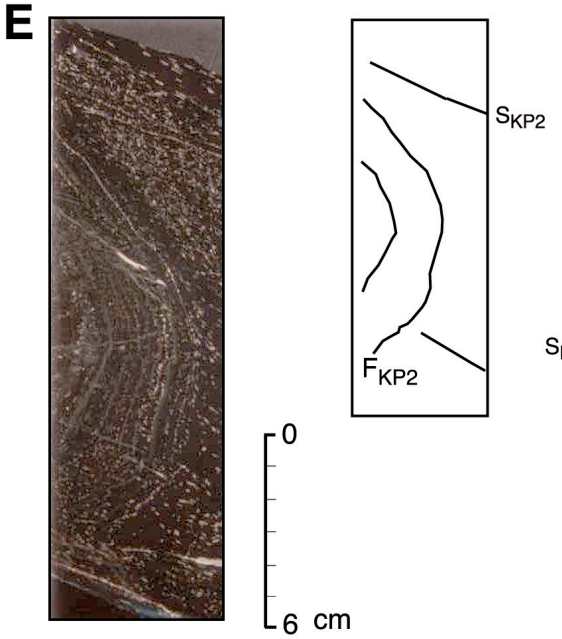
E
S_{KP2}
F_{KP2}
0
6 cm

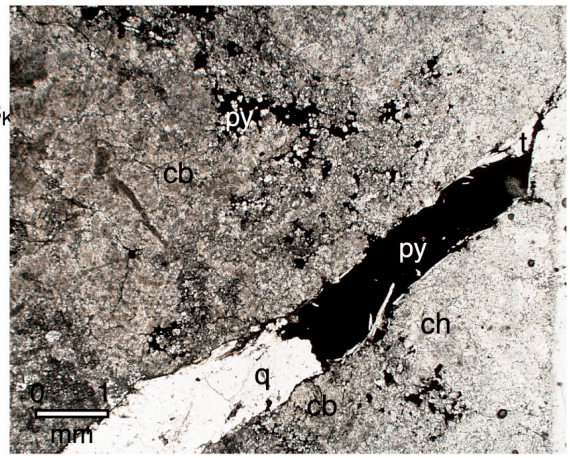
G
py
cb
t
py
ch
q
cb
0
1
mm

Figure 7.7 Features of hydrothermal minerals at Onedin.
(A) Randomly oriented hydrothermal talc flakes (t) surrounded by sphalerite (sp) are much larger than the metamorphic talc (t) found in the upper part of the photomicrograph which defines S_{KP1} and the crenulation cleavage S_{KP2} (KPD 31 264 m, x 50, ppl).
(B) Stubby white mica flakes (w) in an aluminous bed. The flakes are not all oriented in the foliation (S_{KP2}) and some are parallel to bedding (S_0), including some preserved within pyrite (py, KPD 31 177.3 m, x 50, x nicols).
(C) Quartz-bearing mudstone facies from the footwall with quartz crystals (q) surrounded by fine-grained quartz, chlorite (ch) and white mica (w). Metamorphic quartz growing in a quartz pressure shadow (arrow, DDH 16A 76 m, x 25, x nicols).
(D) Small quartz crystals (q) nucleating on volcanic quartz (vq) to form quartz 'eyes' abundant in the quartz-bearing mudstone of the footwall (DDH16A 155 m, x 50, x nicols).
(E) Albite and quartz (al+q) cores of perlitic rhyolite in the Onedin hanging wall overprinted by white mica and chlorite alteration (w+ch, yellowish areas). Perlitic fractures are arrowed. The dark needle-like crystals are probably ilmenite (KPD 32 257 m, x 25, ppl).

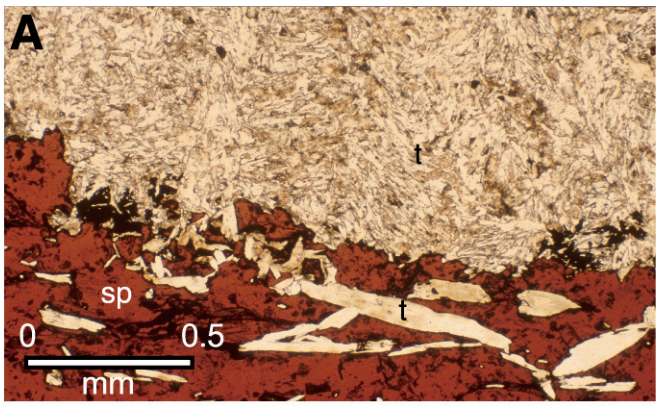
A
t
sp
t
0
0.5
mm

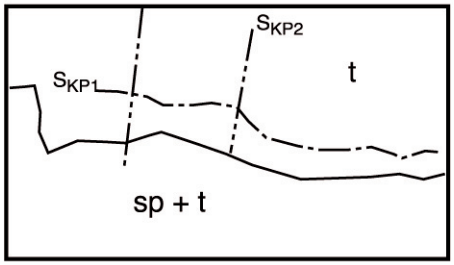
SKP2
SKP1
t
sp + t

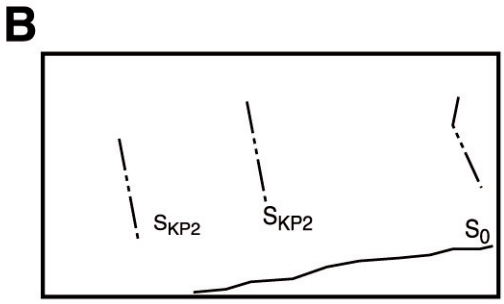
B
SKP2
SKP2
S0

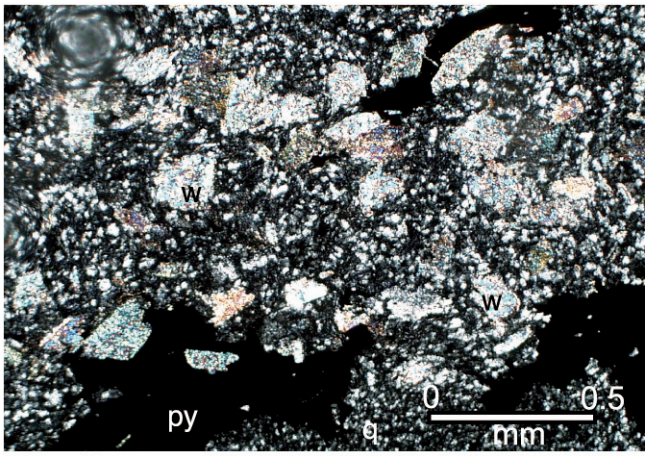
w
w
py
q
0
0.5
mm

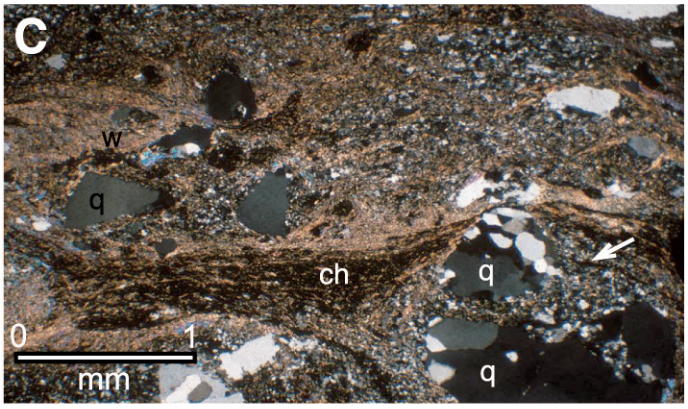
C
w
q
ch
q
q
0
1
mm

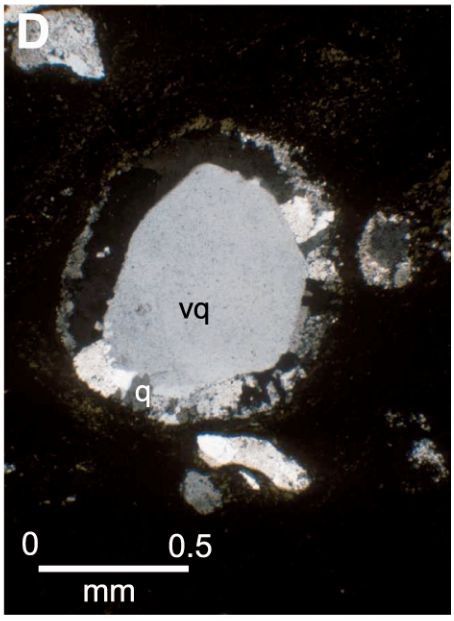
D
vq
q
0
0.5
mm

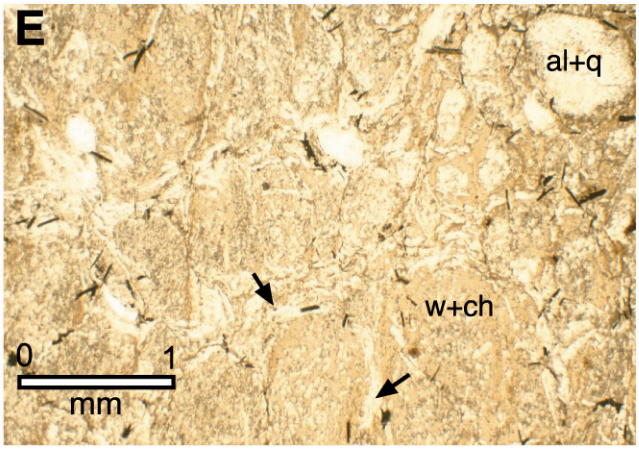
E
al+q
w+ch
0
1
mm

Table 7.1 Element abundances in sphalerite in central part of Onedin.

Sample (No. of analyses) Ore type	**31 210.8** (27) Carbonate-hosted	**31 212** (67) Carbonate-hosted	**32 120.7** (44) Chlorite schist-hosted	**32 329.7** (14) Carbonate-hosted	**32 336** (25) Carbonate-hosted
S Average Range	32.93 32.68 –3 3.12	33.23 33.04 - 33.45	29.52 28.70 – 30.26	33.17 32.82 - 33.32	32.96 32.60 - 33.15
Zn	59.05 58.27 - 59.96	57.47 56.52 - 58.16	57.14 55.95 - 57.85	56.69 56.37 - 57.07	57.49 57.10 -57.72
Mn	0.04 0.03 - 0.05	0.07 0.04 - 0.09	0.03 0.02* - 0.05	0.02 0.02* - 0.05	0.03 0.02* - 0.05
Fe	6.96 6.59 -7.20	7.17 6.74 -7.35	6.71 6.30- 7.10	7.52 7.41 - 7.60	7.11 6.14 - 7.54
Co	0.02 0.02* - 0.03 (n=21)	0.024 0.02* - 0.04 (n=36)	0.02 0.02* - 0.03 (n=3)	0.01 0.02* - 0.03 (n=3)	0.12 0.11 - 0.14 (n=24)
Cu	0.12 0.04*, 0.13 (n=2)	n/s	0.11 0.06 - 0.15 (n=4)	0.07 0.04, 0.08 (n=2)	0.15 0.04* - 0.26 (n=5)
Cd	0.09 0.06 - 0.16 (n=27)	0.19 0.11 - 0 .29 (n=63)	0.15 0.07 - 0.21 (n=13)	0.19 0.13 - 0.24 (n=7)	0.25 0.17 - 0.31
Hg	0.1 0.09, 0.1 (n=2)	0.17 0.10 - 0.29 (n=13)	0.16 0.10 - 0.23 (n=9)	n/s	0.10 0.10 - 0.11 (n=4)

*Lower detection limit (σ_1)
n = number of significant analyses
n/s = no significant results
Se, Ag, Ge, Ga and In tested with no significant results

contain up to 1.7 wt% As. Ni. Zn, Se, Ag and Pb are only present in trace amounts or below detection limits, in the pyrite analysed (Table 7.2).

Chalcopyrite

Chalcopyrite is present in both carbonate- and chlorite-hosted sulfide zones throughout Onedin. In a few intervals it is the dominant sulfide mineral, e.g., KPD 32 329 m, it comprises 80% of the sulfide minerals. Chalcopyrite is commonly less abundant, disseminated as individual crystals and small pods and bands (<0.1 cm across) between sphalerite, pyrrhotite and galena in the carbonate-hosted sulfide (Figs 7.4B, C, D) and with pyrrhotite and pyrite in the chlorite schist–hosted sulfide zones. Some veins contain chalcopyrite in association with quartz (Fig. 7.3C) and chalcopyrite stringers are present in the deeper, central part of the prospect (KPD 36). Late carbonate-rich veins contain chalcopyrite at their margins (Fig. 7.6C).

Galena

Galena is the least abundant sulfide mineral. It is scattered as small interstitial (<0.2 mm) crystals throughout the massive carbonate-hosted and the chlorite-hosted massive sulfide (Fig. 7.4B). It forms layers in some parts of the chlorite schist-hosted sulfide (Fig. 7.6D). Crystals associated with chalcopyrite are on the edges of broad, late carbonate-bearing veins. Most galena have a high proportion of Pb, with only a low abundance of minor elements (Table 7.3).

Table 7.2 Element abundances in pyrite from the central part of Onedin.

Sample (No. of analyses) Ore type	**32 120.7** (4) Chlorite schist-hosted	**32 329** (4) Carbonate –hosted	**32 336** (18) Carbonate –hosted	**32 350.3** (5) Carbonate –hosted	**35 350.8** (9) Chlorite schist –hosted
S Average Range	52.3 52.01 - 52.63	51.73 51.35 - 52.00	52.62 51.65 - 53.42	52.85 52.76 - 53.05	53.43 52.69 - 53.87
Fe	45.95 45.6 - 46.3	46.33 45.9 - 46.5	46.57 45.65 - 47.27	46.62 46.06 - 46.87	46.43 45.73 -47.38
Co	0.05 0.04*, 0.06 (n=2)	n/s	0.05 0.04* - 0.12 (n=8)	n/s	0.69 0.13 - 1.25 (n=5)
Ni	0.12 0.02* - 0.14 (n=3)	n/s	0.06 0.02* - 0.14 (n=5)	0.03 0.03, 0.35 (n=2)	0.03 0.02*, 0.03 (n=2)
Zn	0.34 0.2 , 0.9 (n=2)	n/s	0.28 0.17 -0.37 (n=3)	n/s	n/s
As	n/s	0.80 0.40 - 1.73	0.15 0.04 - 1.04 (n=5)	n/s	0.10 0.01 - 0.19 (n=6)
Se	0.03 0.01* - 0.14 (n=3)	n/s	0.03 0.01* - 0.04 (n=8)	0.027 (n=1)	0.03 0.01* - 0.07 (n=4)
Ag	n/s	0.07 (n=1)	0.06 0.05 - 0.09 (n=4)	0.07 (n=1)	0.09 0.06 - 0.12 (n=3)
Pb	0.25 0.22 - 0.29 (n=3)	0.25 0.10* - 0.45 (n=3)	0.26 0.12 - 0.38 (n=12)	0.26 0.21, 0.32 (n=2)	0.26 0.10* -0.36 (n=7)

All results reported in wt %.
* Lower detection limit (σ_1)
n = number of significant analyses (above σ_1).
n/s = no significant results

The galena analysed for minor elements are all from the carbonate-hosted massive sulfide lenses of the central part of the Onedin prospect (Table 7.3). Little Bi is in the galena analysed, except in KPD 32 329m where it forms 0.4 wt% of the galena. Ag and Sb are depleted, with Ag up to 0.8 wt% and Sb up to 0.7 wt% in some galena. Samples with the most abundant Ag also contain the most abundant Sb. Se is absent in the galena from KPD 31, but up to 1.1 wt% in galena from KPD 32.

Freibergite

Freibergite (Cu, Zn, Fe)$_8$Sb$_2$S$_7$ is a fahlore which accompanies galena and pyrrhotite in the high Ag zones of the KPD 31 (KPD 31 210.8, 212 m). Crystals are rounded, less than 0.1 mm across and interstitial to sphalerite. No samples were preserved from DDH 1 206–211 m to test which minerals contain the high silver values in this interval (580 ppm Ag).

Table 7.3 Element abundance in galena from the central part of the Onedin prospect.

Sample (No. of analyses) Ore type	**31 210.8** (18) Carbonate-hosted	**31 212** (21) Carbonate-hosted	**32 329** (21) Carbonate-hosted	**32 336** (23) Carbonate-hosted
S Average Range	12.78 12.28 - 13.15	13.17 12.57 - 13.64	13.67 12.56 -13.24	12.96 12.77 - 13.15
Pb	82.80 81.88 - 83.62	83.56 81.14 - 85.11	79.78 82.81 - 85.57	83.05 81.73 -84.11
Se	1.04 (n=1)	0.01* (n=1)	0.34 0.06 - 1.11	0.03 0.01* - 0.10
Ag	0.09 0.04 - 0.16	0.14 0.08 - 0.22	0.22 0.02* - 0.31 (n=20)	0.19 0.02* - 0.79 (n=22)
Sb	0.19 0.02* - 0.15 (n=16)	0.08 0.04 - 0.16	0.08 0.02* - 0.16	0.21 0.02* - 0.72 (n=20)
Hg	0.05 0.07* - 0.09 (n=15)	0.11 0.07* - 0.16 (n=6)	0.04 0.07* - 0.10 (n=18)	0.05 0.07* - 0.09 (n=22)
Bi	0.25 (n=1)	n/s	0.34 0.25 - 0.44 (n=14)	n/s

All results in wt%
*Lower detection limit (σ_1)
n= number of samples above detection limit (σ_1).
n/s = no significant results

Discussion

Slightly reduced abundances of FeS in sphalerite of the chlorite schist-hosted sulfide zones (10 mol%) compared with sphalerite of the carbonate-hosted sulfide zones (10–13 mol wt%) may reflect slightly higher $a(S_2)$ in the fluid which deposited the chlorite schist-hosted sulfide zones. A variation in the $a(S_2)$ of the fluids depositing the sulfide minerals in these different host units is consistent with the predominance of pyrrhotite in the carbonate-hosted sulfide zones and pyrite in many parts of the chlorite schist-hosted sulfide zones (Toulmin & Barton 1964, Scott & Barnes 1971, Czamanske 1974).

Cd levels (0.06–0.31 wt% Cd) in sphalerite from Onedin are comparable to the Cd content of other Australian VHMS deposits (0.06–0.29 wt% Cd) (Groves & Loftus-Hills 1968, Huston et al. 1995a). Cobalt is only elevated in the sample associated with abundant Cu in sphalerite at KPD 32 336 m. This sample only contains minor chalcopyrite (Fig. 7.4B).

Se in pyrite is thought to be an indicator of the origin of hydrothermal fluids (Loftus-Hills & Solomon 1967, Huston et al. 1995a). The abundance of Se in pyrite at Onedin, cannot be fully evaluated as Se in many pyrite samples are below the Se-detection limit on the microprobe (0.01 wt%). The most abundant Se in pyrite is about 0.07 wt%, comparable to the Se abundance in pyrite from the footwall stringer zone of Dry River (0.076 wt%), the most elevated value for eastern Australian VHMS deposits (Huston et al. 1995a). Generally, such high Se values in pyrite are thought to be associated with Cu-rich deposits and an indicator of magmatic input. Onedin is not a particularly Cu-rich deposit (1% Cu). The elevated Se-levels in pyrite may be caused by early precipitation of the pyrite, prior to the formation of galena, which also incorporates Se into its

lattice, from acidic hydrothermal fluids (Huston et al. 1995a). The pyrite with high Se is a nodular mass rather than the later cubic form of pyrite. Several galenas have high Se-levels (Table 7.3). In samples where both galena and pyrite have been tested for Se, the Se is in the galena, but below detection limits for pyrite, e.g., KPD 32 329 (Tables 7.2, 7.3).

Some pyrite grains from the carbonate-hosted sulfide zones have elevated As (< 1.73 wt%). These pyrites are generally recrystallised and so the As must be within the pyrite lattice, rather than present as arsenopyrite inclusions.

Co/Ni ratio in pyrite has been used to determine the sedimentary (consistently <1) or hydrothermal origins (highly variable, >1) of some pyrite (Bralia et al. 1979, Raymond 1996). Although Co and Ni are above detection limits for many of the pyrite analysed, only one sample has both Co and Ni above detection limits (Co/Ni=0.27, KPD 32 120 m), which in isolation cannot be interpreted.

7.2.4 METAL ABUNDANCES AT ONEDIN

Analyses of massive sulfide intervals were provided by Billiton Australia for DDH 5, KPD 31, 32, 34, 35 and 36. These analyses have been averaged over intersected massive sulfide intervals (Appendix 9). Analyses for the drillcore from DDH 1 and DDH 22 was completed by Kennecott (1973).

The sulfide zones at Onedin are dominated by Zn (<30 wt%) with less Cu (most <5 wt%) and Pb (up to 4 wt%, Figs 7.2, 7.8). Metal ratios show covariance, with Pb/Zn close to 5 (Fig. 7.8). Correlation between either of these metals and Cu is poor (Fig. 7.8). Samples from the southern end of the deposit provide the highest relative proportion of Pb to Cu, or Pb to Zn, and only four samples have Cu/Zn ratios greater than one (KPD 32, 318, 319 m, DDH 5 120 m and DDH 22, 449 m). Although Cu is found throughout the ore lenses, there are few intervals dominated by Cu, and no obvious Cu-rich zones as reported from some VHMS deposits, e.g., Kuroko (Ohmoto 1996), Rosebery, Mt Chalmers and Scuddles (Large 1992). Comparisons of the Cu and Pb, and Zn and Pb with modern black smokers indicates that the system at Onedin was not particularly depleted in Pb, and plots close to the average Kuroko deposit value in the Cu versus Pb plot (Fig. 7.8B) and with similar Pb values, albeit lower Zn values than many of the deposits in backarc basins (Fig. 7.8C). All zinc ratios (ZR=100Zn/Zn+Pb) of assays (with Zn and Pb > 300 ppm) from Onedin drillcore are greater than 60 (Fig. 7.9), with the exception of one near-surface sample from DDH 1 24.4 m (ZR=48). This sample may have been oxidised. The frequency distribution pattern of the ZR at Onedin are dissimilar to that for sediment-hosted massive sulfide deposits, but similar to that of VHMS deposits (Huston & Large 1987) (Fig. 7.9).

With the exception of one interval, all the massive sulfide analysed at Onedin fall into the Zn-Pb-Cu type and Zn-Cu type of VHMS deposit (Solomon 1976) (Fig. 7.2).

Most samples contain less than 200 ppm Ag, although one interval from near the bottom of DDH 1 (206–211 m) contains 580 ppm. Silver levels show moderate correlation with Zn and Pb, but are independent of Cu (Fig 7.8D-F). For example, the interval at KPD 31 210–214 m, which has the highest Zn (30.2 %) and the second highest Pb (5.67%) value of the assayed samples also has high Ag (323.6 g/t). Cu in this interval is only 0.13 %.

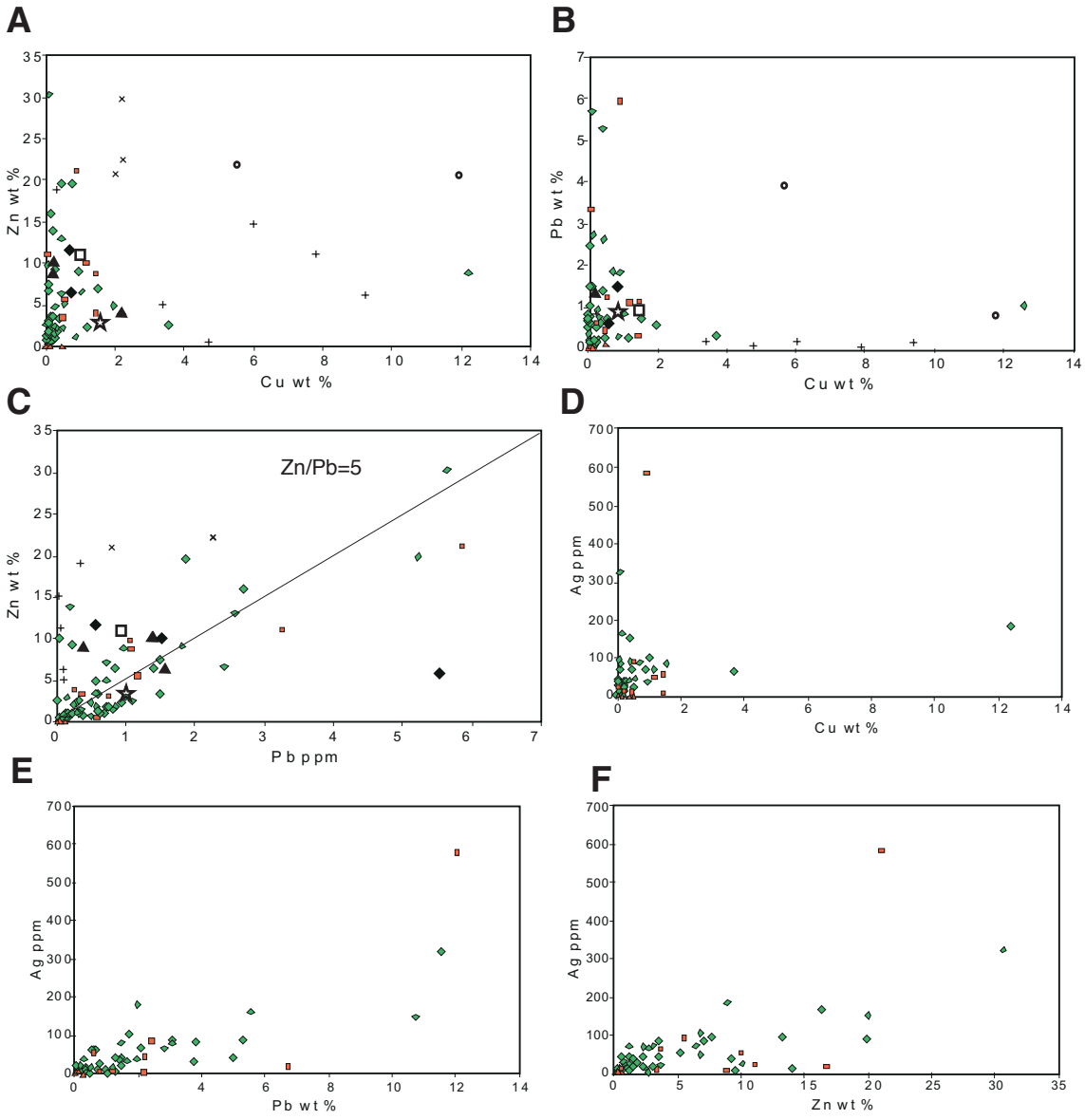

Figure 7.8 Metal abundance covariance plots for samples assayed at Onedin. A-C are the main base metal ratios and also show averages for Onedin and Kuroko deposits (Ohmoto & Skinner 1983) as well as other modern black smoker deposits from mid-ocean ridges, forearc and some backarc settings (Iisaza et al. 1999). Also depicted are averages for some Palaeoproterozoic VHMS deposits from Canada Bernier & MacLean 1993, Syme & Bailes 1993, Galley et al.1993) and Scandinavia (Isokangas 1978, Hedstrom et al. 1989, Duckworth & Rickard 1993). Plots D-F show the variation in Ag abundance with the main base metals.

- Onedin North
- Onedin Central
- Onedin South
- Average Onedin
- Average Kuroko deposits
- Mid-ocean ridges
- Forearc
- Backarc
- Proterozoic Canada
- Proterozoic Fennoscandia

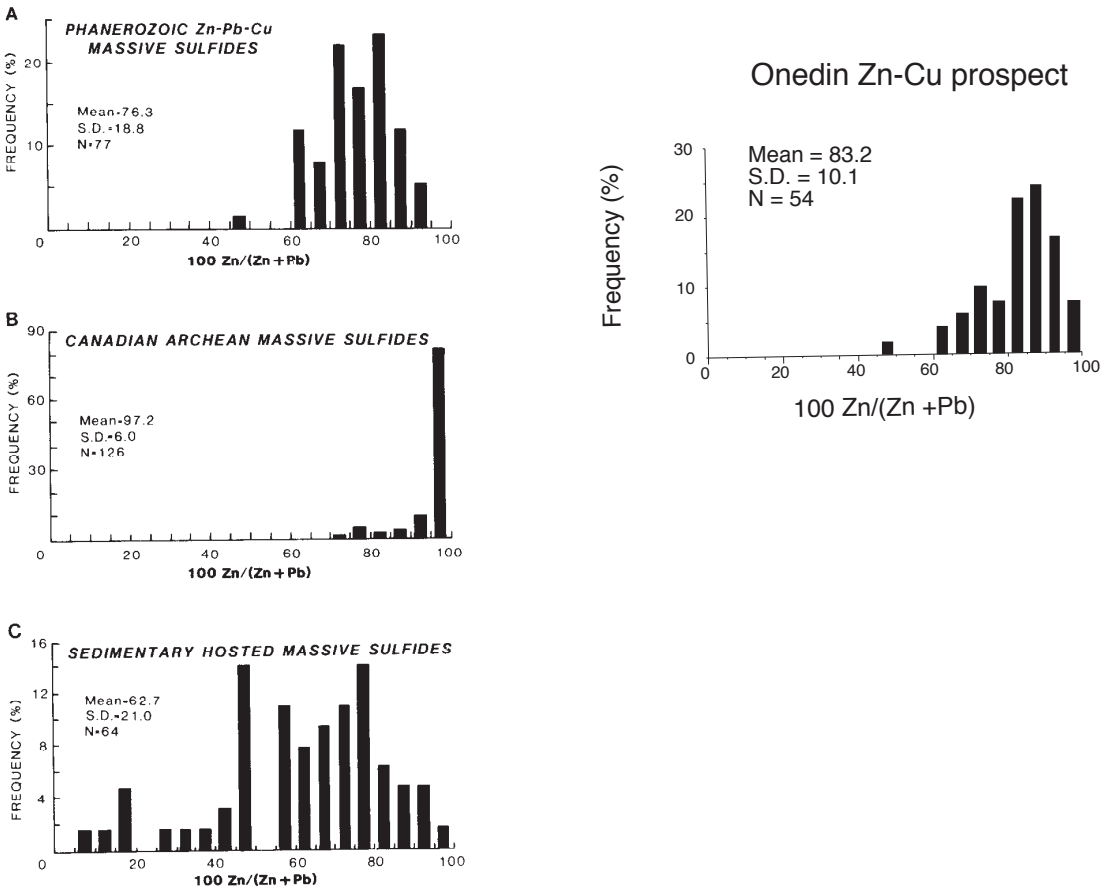

Figure 7.9 Zinc ratio (ZR= 100Zn/(Zn+Pb)) frequency plot from assay data for Onedin compared with zinc ratio frequency plots for (A) Phanerozoic VHMS deposits, (B) Canadian massive sulfide deposits, and (C) sedimentary hosted massive sulfide deposits (all from Huston & Large 1987). The pattern for the Onedin data is very different to the spread of zinc ratios in the sedimentary hosted massive sulfide deposits. It is similar to the plot for Phanerozoic VHMS deposits, but has a higher mean and lower standard deviation. The mean is between that of the Canadian Archaean deposits and Phanerzoic deposits

The pattern in fault-related metal values suggest that there was limited remobilisation associated with some faults. Portions of the massive sulfide lenses cut by brittle structures display a significant upgrading in metal values from the surrounding values. For example, a fault at KPD 32 102–11 m has elevated Zn and Ag (10% Zn, 26g/t Ag) relative to the surrounding chlorite schist-hosted sulfide zone (0.8% Zn, 4.94 g/t Ag, Fig. 7.5). Cu grade (0.04%) is unaffected by this fault. However, abundant sulfide minerals are not in faults away from broader sulfide zones, and metal values are not upgraded by all faults (Fig 7.5).

Discussion

The sulfide zones at Onedin lack copper-rich and zinc-rich zones. The Cu is distributed throughout the zones in varying abundances and Pb is also present in varying amounts. The annealed textures in the main sulfide zones preclude an extensive investigation of the paragenesis of the sulfide minerals. Timing of the sulfide mineral deposition cannot be constrained. However, covariance of the Pb, Zn and Ag suggests that these metals may have been deposited together. The relationship with chalcopyrite is less certain. It may have been deposited with, or overprint, the sphalerite-rich sulfide zones, but it is unlikely that Cu was associated with the late brittle fractures.

Although the ZR is high (av. 83.3) at Onedin, the plots of Pb against Cu and Zn reveal that average Pb abundance at Onedin is similar to Pb abundance for averaged Kuroko deposits. The sulfide zones at Onedin may be better thought of as Zn-rich, rather than Pb-poor. Abundant Zn at Onedin may be related to the A-type felsic volcanic rocks present in the KPF, a relationship recognised by Lentz (1998a) in several VHMS districts.

7.3 EFFECTS OF DEFORMATION AND METAMORPHISM ON THE SULFIDE ZONES

Metamorphism and deformation have affected the sulfide zones at Onedin. Evidence of recrystallisation and mobilisation of the main sulfide minerals is abundant at all scales. No primary features, such as pyrite framboids or spheres were observed, but some textures indicative of radiating or open-space-fill are present. Veining is common. New mineral growth during metamorphism, is evident in crenulated patches of chlorite, biotite, talc and tremolite. Pyrite is common in fold-hinge foliations (Fig. 7.6E) and late pyrite cubes enclose recrystallised sphalerite and aligned minerals (Fig. 7.6B).

Late sphalerite+carbonate veins cut through areas dominated by chlorite or quartz+ chlorite. Many are up to 0.2 m wide, with only one edge observed in core. In one example, they cross-cut a small F_{KP2} fold formed in chlorite (Fig. 7.6C). Chalcopyrite and some galena at the edges of these veins indicate high heat flow at the margin. The vein interiors are dominated by sphalerite + carbonate.

Fractures and dilation areas formed during deformation, created space between competent blocks, allowing the infiltration of some sulfide minerals. The minerals include chalcopyrite, sphalerite, galena and pyrite. These are associated with carbonate, chlorite and talc. Other textures are described below.

7.3.1 LAYERING

Within and on the edges of the carbonate-hosted sulfide zones, layers (1–2 mm thick) of aligned gangue minerals such as talc, quartz and carbonate, alternate with layers of sphalerite, pyrrhotite, minor chalcopyrite and galena. In the chlorite schist-hosted sulfide zones, broad layering consists of pyrrhotite-dominated layers alternating with thin galena-rich bands (<2 cm thick) and pyrite-rich bands (Fig. 7.6D). This banding may be related to, or enhanced by, deformation (D_1 and D_2), metamorphism and accompanying sulfide remobilisation.

7.3.2 FOLDING

Layers of sulfide minerals including sphalerite, pyrrhotite, chalcopyrite and pyrite, are folded around F_{KP1} and F_{KP2} folds (Fig. 7.6E, F). In some places, the sulfide minerals have been recrystallised into the direction of the foliation of a fold structure (Fig. 7.6E). Veins containing sphalerite have also been folded by F_{KP2}.

7.3.3 SULFIDE REMOBILISATION TEXTURES

Where massive sulfide minerals, such as sphalerite surround platy minerals, such as talc and chlorite, deformation has caused the sulfide minerals to flow around the platy minerals. This movement is evident from folding and/or internally kinking of the platy minerals (Fig. 7.6A, F). Harder sulfide minerals, such as pyrite were rounded by rotation and movement of surrounding softer sulfide minerals, such as pyrrhotite, chalcopyrite or sphalerite. These features probably relate to the early ductile deformations (D_1 and D_2).

7.3.4 SHEARING

Shearing has affected veins and dilation zones during compression. The high competency contrast between the sulfide minerals and their less competent hosts, has focussed deformation into the sulfide mineral layers. The result are discontinuities and zones (<0.1–5 mm across, Fig. 7.6F), where the sulfide minerals form thin (<0.1 mm) layers, aligned with the surrounding talc, chlorite, carbonate or quartz crystals. Shearing is part of the early ductile deformation events, and probably closely associated with D_2 (Chapter 3).

7.3.5 PIERCEMENT VEINS

Many late stage milky quartz veins terminate in forked areas or piercements, which are filled by pyrite, pyrrhotite or chalcopyrite. Some piercement veins may be related to late stage brittle movement, cross-cutting both S_{KP1} and S_{KP2} (Fig. 7.6G). The milky quartz attests to fluid involvement in the remobilisation of these sulfide minerals.

7.3.6 CATACLASIS OF BRITTLE SULFIDE MINERALS

Brittle fractures are abundant in pyrite grains and massive pyrite patches (Fig. 7.6D). Extensional microfractures between the pyrite are filled by chalcopyrite and pyrrhotite. This texture is consistent with cataclastic deformation of pyrite and mechanical, or solution transfer of the other sulfide minerals into the fractures. Similarly fractured magnetite are surrounded by talc and carbonate, which have grown within microfractures, during metamorphism.

7.4 ALTERATION HALO AT ONEDIN

The distribution of altered rocks at Onedin appears to be semi-conformable with the major units. The footwall is dominated by quartz-bearing mudstone facies containing quartz, some paragonite or muscovite and abundant chlorite, with talc, pervasive quartz and pyrite near the host sequence. The quartz in some mass flow units is blue and cloudy close to the massive sulfide zones. In the host sequence, altered rocks contain chlorite with talc, tremolite, carbonate, biotite and quartz. In the hanging wall rhyolite, chlorite and white mica are still major components along with albite and quartz.

Altered rocks at Onedin are made up of chlorite + carbonate + talc + quartz ± white mica ± tremolite/actinolite ± biotite/phlogopite ± albite + ilmenite + sphene.

7.4.1 PARAGENESIS AND OVERPRINTING RELATIONSHIPS

Given the greenschist metamorphic grade of the rocks at Onedin, distinguishing between minerals grown during alteration or metamorphism is problematic. Despite this, some forms of chlorite, carbonate, talc and white mica are identifiably pre-deformational. Hydrothermal talc crystals are large (0.8 mm long) and locked in random orientation in massive sphalerite (Fig 7.7A). Hydrothermal white mica are large, stubby crystals (0.6 mm x 0.3 mm, Fig. 7.7B), distinct from the smaller (0.05 mm x 0.01 mm), flakes of white mica aligned with the metamorphic foliations (Fig. 7.7C). However, most assemblages display features consistent with growth during metamorphism. Tremolite/actinolite crystals cut across both foliations in places and most talc, chlorite, phlogopite and white mica define foliations (S_{KP1}, S_{KP2}). The paragenesis of the main minerals at Onedin is summarised in Figure. 7.10 and individual minerals and their chemistry are documented in the following section.

7.4.2 ALTERATION MINERALS AND MINERAL CHEMISTRY

Chlorite

Chlorite occurs in association with talc and carbonate in the chlorite schist-hosted sulfide zones, below the upper carbonate lens and is the most common mineral along with quartz in the footwall. Chlorite fills broad veins. These veins were major fluid pathways, evident from the formation of sphene and ilmenite. These minerals formed as mobile elements were removed and immobile elements, such as titanium, became concentrated. The chlorite zones can be overprinted by two foliations, S_{KP1} and a crenulation cleavage (S_{KP2}). Both are defined by chlorite.

The chlorite analysed display a range of FeO and MgO compositions (Fig. 7.11A). Ripidolite is most common, with pycnochlorite, clinochlore and minor sheridanite (Appendix 4). Some variation may be due to metamorphic overprinting. The most iron-rich samples come from the footwall (Fig. 7.11A) and the most magnesium enriched samples from close to the carbonate-hosted massive sulfide lenses in the host sequence.

Footwall chlorite can be iron or magnesium rich, as displayed in the shortwave infra-red (SWIR) spectra of drillcore through the footwall in DDH 16A and KPD 35 (Fig. 7.12). Although there is an overall change from iron-rich chlorite distal to the host sequence (e.g., KPD 35 88 m) to Mg-rich chlorite in the host sequence (e.g., KPD 35, 182 m), the Mg-Fe chlorites of the footwall display no systematic change in Mg/Fe ratio towards the host sequence as reported from some VHMS deposits (Urabe et al. 1983).

Carbonate

Carbonate is the most common host for sulfide minerals at Onedin. Detailed descriptions and analysis of the carbonate is presented in Chapter 8 and only a summary of some main points is presented here. Carbonate alteration is thickest in the host sequence of the central and northern part of Onedin and thins rapidly even 50 m further north. Thirteen petrographically distinct carbonate types formed during sedimentation, diagenesis, alteration, metamorphism and deformation. These include spheroids, zoned dolomite rhombs, laminated and bladed dolomite crystals, massive carbonate and recrystallised dolomite, to name a few. Analyses of the carbonate, indicates that most are dolomitic. Many are iron-rich dolomite and there is minor ankerite

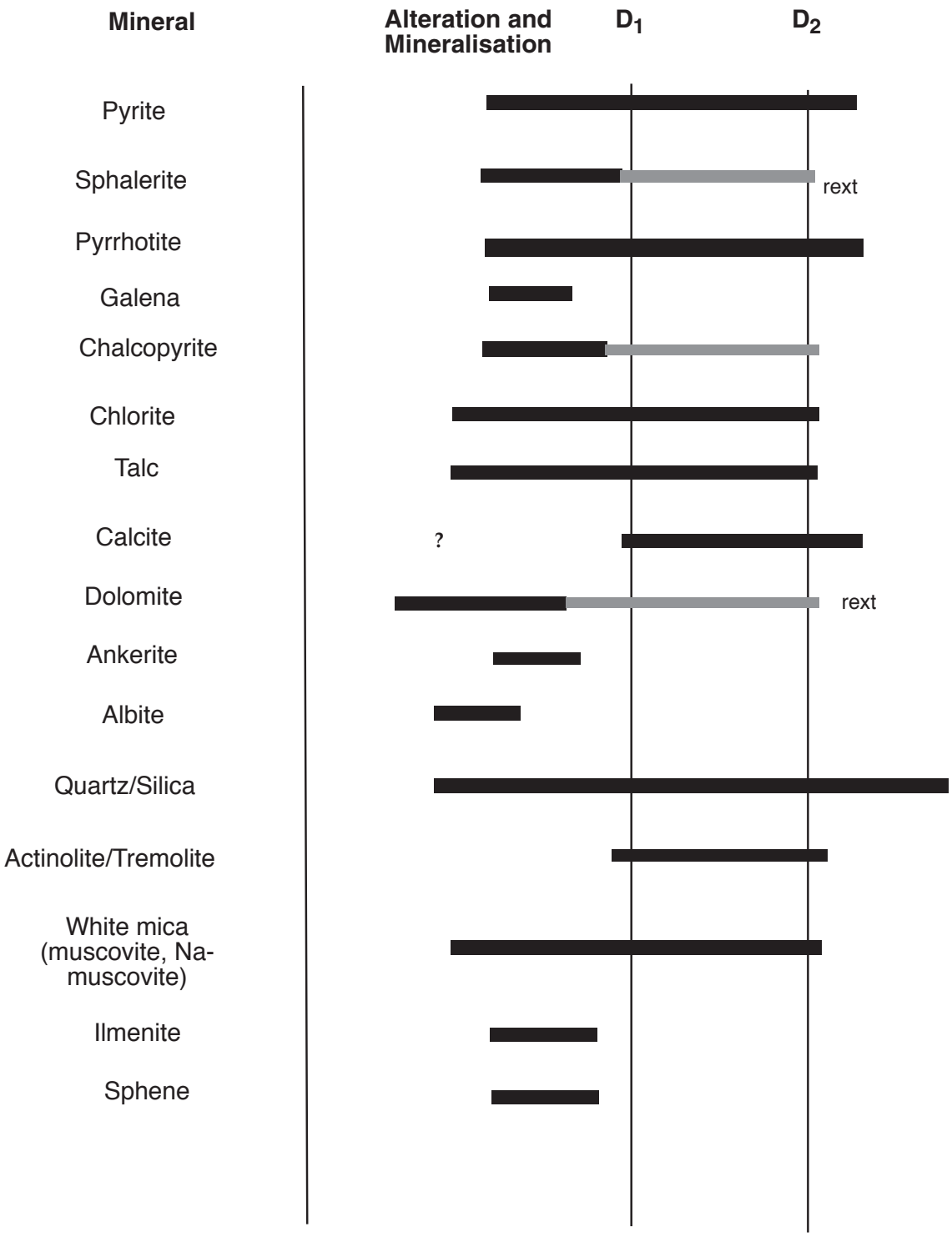

Figure 7.10 Paragenetic sequence of mineral growth in relation to alteration, mineralisation and deformation ($D_1$and D_2) at Onedin. Metamorphism has annealed early textures in the sulfide minerals, so it is assumed that these minerals initially deposited during the same mineralising phase.

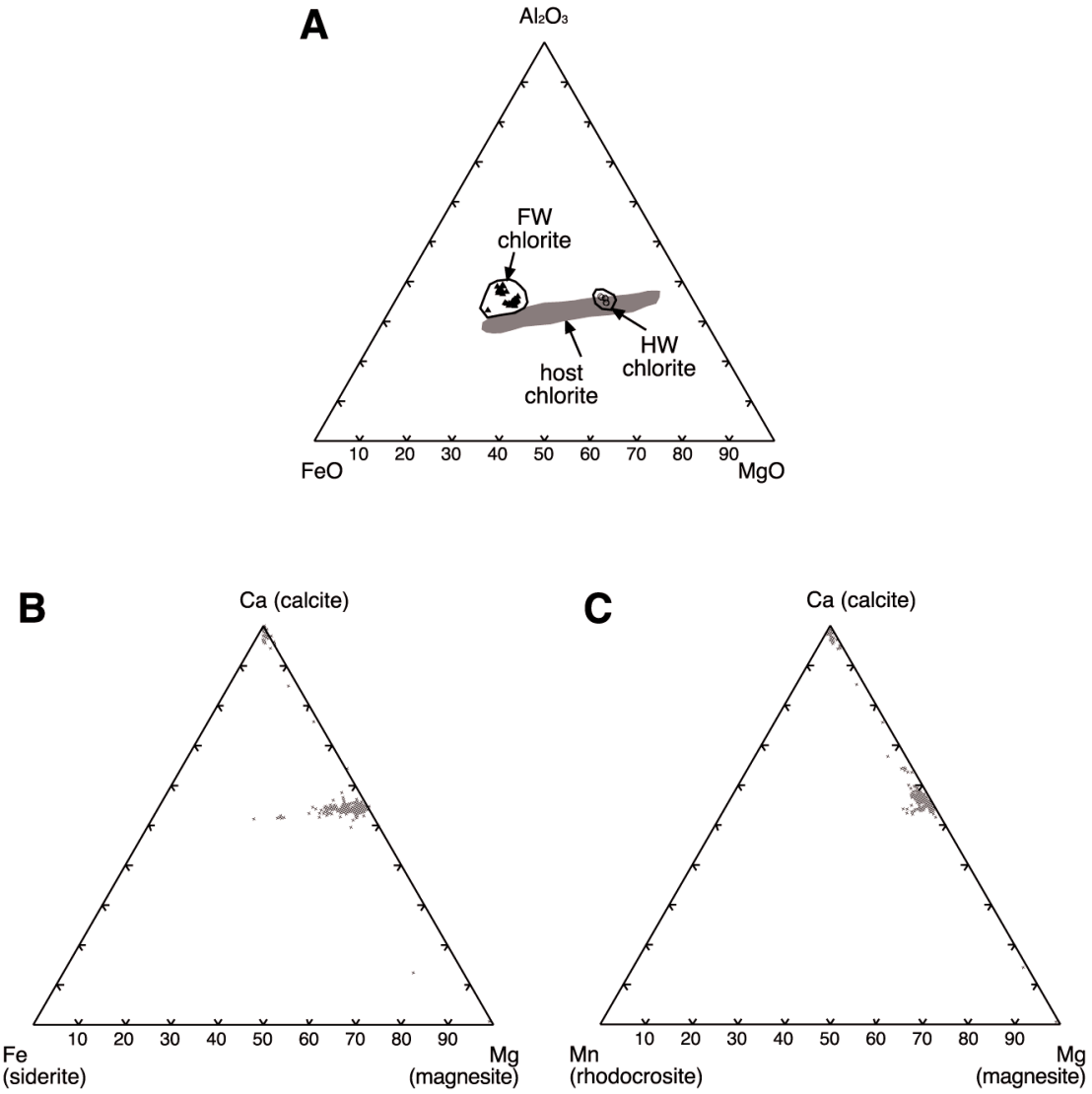

Figure 7.11 (A) Al_2O_3-FeO-MgO triplot of the chlorite compositions from the footwall, host sequence and hanging wall at Onedin. The host sequence contains the most Mg-rich chlorite and the footwall contains chlorite with the highest Fe content. (B) Fe-Ca-Mg carbonate composition from carbonate host to sulfide zones. (C) Mn-Ca-Mg carbonate composition from host sequence to sulfide zones.

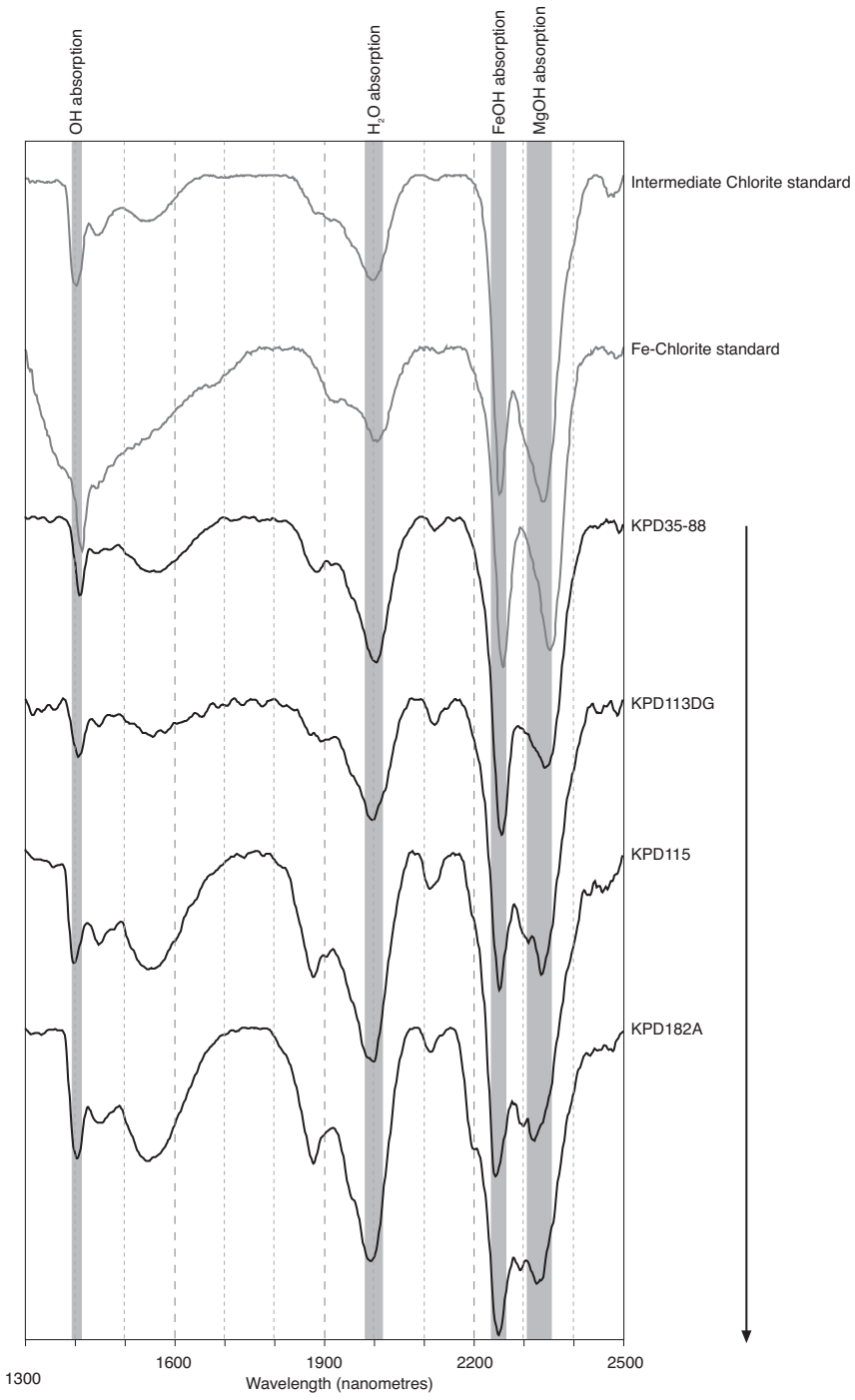

Figure 7.12 PIMA spectra of chlorite in footwall samples. The top two spectra are a reference of intermediate chlorite with mixed FeOH and MgOH and Fe-rich chlorite. The following four spectra are from the footwall in KPD 35. The arrow indicates direction towards the sulfide zones. The sample closest to sulfide zones appear to have the highest Mg content.

(Fig. 7.11B), but manganese content of the carbonate is low (less than 5% $MnCO_3$, Fig. 7.11C). Metamorphic carbonate is calcite or ferroan calcite.

Carbonate appears to be a replacement of early carbonate-bearing mudstone and glass, evident in preservation of small, early dolomite rhombs and vitriclastic textures (Chapter 8, Fig. 8.2A, B).

Talc

Most clear, elongate minerals near the sulfide zones at Onedin are talc. Talc occurs within the footwall and just below the sulfide zones, as well as associated with and near the margins of carbonate lenses. It is absent from the hanging wall. Talc at Onedin accommodates up to 7 wt% iron oxide (Appendix 4). The iron-rich samples may contain ferrous talc or minnesotaite. X-ray diffraction was not used to distinguish these phases.

Early alteration talc forms large crystals (up to 0.8 mm long and 0.1 mm wide), which are randomly oriented within sphalerite patches. These early talc crystals were kinked by later deformation (Fig, 7.6A). The talc enclosed by sphalerite are significantly larger than the metamorphic talc grown in the cleavage and crenulation cleavages (up to 0.1 mm long and 0.02 mm wide, Fig. 7.7A). Chlorite can be inter-grown with talc, and spots of talc within chlorite occur in transition areas between talc-dominated and chlorite-dominated zones. Sphalerite and carbonate are commonly associated with talc in the massive sulfide zones.

White Mica

White mica occurs in the footwall, host sequence and hanging wall. SWIR spectral analysis of footwall samples suggests that the white micas in the footwall have AlOH adsorption features at wavelengths below 2200 nM (Fig. 7.13). In other VHMS systems, similar responses in SWIR spectra were consistent with sodic muscovite (Herrmann et al. 2001). These authors suggested that low values for AlOH adsorption in SWIR spectra (2194-2204 nM) indicate non-phengitic white mica, with sodic muscovite at the low end of the range. The SWIR spectra indicate muscovite dominates close to the host sequence (Fig. 7.13). In the hanging wall, white mica is associated with chlorite. Nearly all the white micas are part of the metamorphic assemblage forming in pressure shadows and aligned with the main cleavage and crenulation cleavage (Fig. 7.7C). Some stubby white mica crystals, present in the host sequence (Fig. 7.7B) may be minerals which grew during hydrothermal alteration. The stubby white micas are 0.6 mm x 0.3 mm, at least an order of magnitude larger than metamorphic white mica (0.05 mm x 0.01 mm).

Quartz

Quartz-dominated patches occur throughout the footwall, but are more abundant near the top of quartz-bearing mudstone. Quartz-dominated areas contain pyrite, minor sphene, some ilmenite, and minor chlorite and are often studded with recrystallised volcanic quartz crystals. The recrystallised volcanic quartz crystals are cloudy and blue in hand specimen. The intensity of the blue colour increases towards the base metal sulfide zone. In quartz-rich patches, the quartz crystals (<0.1 mm across) display straight to irregular, non-sutured boundaries. Embayed volcanic quartz crystals and polycrystalline quartz aggregates (<3 mm across) are surrounded by a dusty halo (<0.2 mm wide) of fine-grained (<0.1 mm) quartz (Fig. 7.7D).

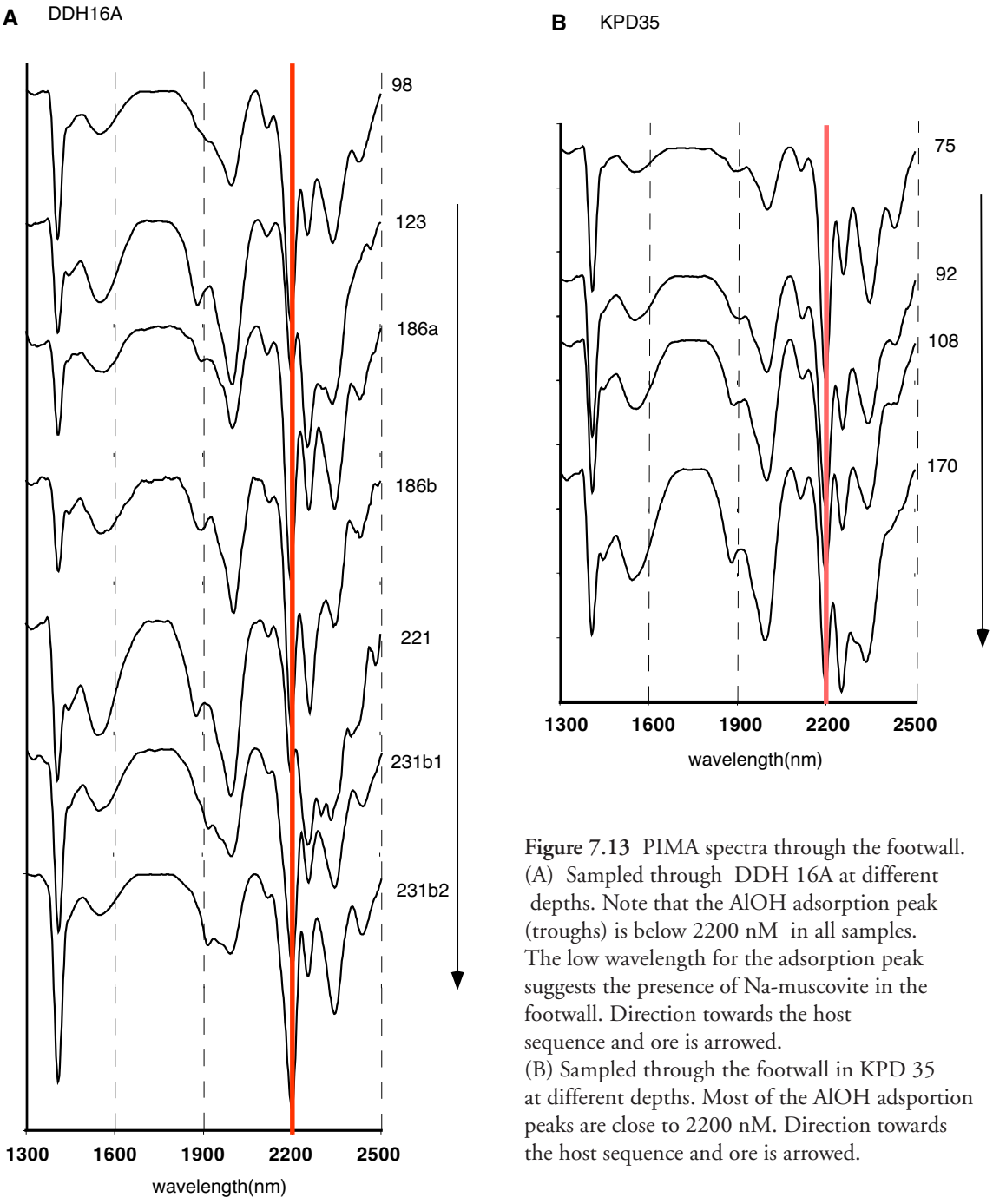

Figure 7.13 PIMA spectra through the footwall. (A) Sampled through DDH 16A at different depths. Note that the AlOH adsorption peak (troughs) is below 2200 nM in all samples. The low wavelength for the adsorption peak suggests the presence of Na-muscovite in the footwall. Direction towards the host sequence and ore is arrowed.
(B) Sampled through the footwall in KPD 35 at different depths. Most of the AlOH adsportion peaks are close to 2200 nM. Direction towards the host sequence and ore is arrowed.

In the host sequence, quartz-dominated rock is commonly associated with sulfide minerals. Recrystallised, silicified "fragments" surrounded by a matrix of carbonate, exits within sphalerite-rich, breccia zones, near the margins of the carbonate-hosted massive sulfide. Silicified sedimentary rocks host cross-cutting, talc, carbonate and sulfide veins in the chlorite schist-hosted sulfide lenses between and above the carbonate lenses. Quartz-dominated bands (< 5 cm thick) occur between mudstone beds in the host sequence above the upper carbonate lens This alteration facies is conformable to bedding in some of the turbidite units.

In the hanging wall, quartz is associated with albite in the cores of perlite (Fig. 7.7E), and forms spherulites, infills perlitic fractures and is abundant in the groundmass.

Quartz has also grown during deformation and metamorphism, evident from quartz crystals in the pressure shadows of large or split volcanic quartz crystals (Fig. 7.7C).

Albite

Albite is associated with quartz in the hanging wall at Onedin. Albite+quartz is locally overprinted by phyllosilicate minerals. The early albite+quartz occupies the cores of perlite, with chlorite, quartz or chlorite and white mica, altering the rock along perlitic fractures (Fig. 7.7E). Probe analyses of the feldspar indicate that these are almost pure albite, with less than 2.6% anorthosite (Appendix 4).

7.4.3 THE GEOCHEMISTRY OF THE ALTERATION HALO

Methods

Two drillholes, DDH 16A and DDH 3, provide a composite section through the footwall, host sequence and hanging wall at Onedin. DDH 16A passed through 280 m of the footwall to finish at the base of the host sequence. It penetrated rhyolite (42 m), then quartz-bearing mudstone facies with some intervening mudstone, and quartz sandstone and mudstone near the top (265 m and 274 m respectively). These lithologies are cross-cut by a mafic dyke (236 m). Twelve geochemical samples were taken at intervals throughout this drillhole. DDH 3 drilled through 338 m of hanging wall and 87 m of the host sequence to end in the top of the footwall. The hanging wall is composed of rhyolite and minor mudstone. Sandstone and mudstone, as well as minor ironstone and carbonate, comprise the host sequence. Samples were taken every 50 m through the hanging wall and at closer intervals in the host sequence.

All samples were analysed for major elements and a suite of trace elements by AMDEL using ICP-MS. Precision is within 10–20% for all the trace elements and 0.01 wt% for major elements (Appendix 7).

Results

The results of the geochemical analyses are tabulated in Appendix 6 and plotted on Figure 7.14. The degree of hydrothermal alteration a rock has undergone can be calculated from the rock geochemistry. The best known measure is the Alteration Index (AI, Ishikawa et al. 1976) based on sericite and chlorite alteration of feldspar and glass in volcanic units:

$$AI = \frac{100\ (MgO + K_2O)}{MgO + K_2O + Na_2O + CaO}$$

Another useful index is the chlorite-carbonate-pyrite index (CCPI) for rocks which display chlorite alteration and contain carbonate (Large et al. 2001):

$$CCPI = \frac{100\ (MgO + FeO)}{(MgO + FeO + Na_2O + CaO)}$$

where FeO is total ($FeO + Fe_2O_3$).

Both AI and CCPI have been calculated for the sampled intervals in DDH 16A and DDH 3 and are also plotted on Figure 7.14.

Footwall

The AI and CCPI are both greater than 80 in most of the footwall sampled (Fig. 7.14), indicating that these rocks experienced intense alteration.

The thickest footwall lithology is the quartz-bearing mudstone facies (Chapter 4). It is sampled between 65 m and 210 m and again at 250 m and is cut by a mafic dyke (236 m). In this unit (65–210 m), most oxides (SiO_2, TiO_2, Al_2O_3, MnO, P_2O_5) display flat abundance patterns (Fig. 7.14). The pattern for CaO abundance is also flat, with the exception of a spike at 90 m, which may represent a vein. Na_2O and K_2O display mirroring patterns, even though the overall amount of Na_2O in the footwall is low (0.21 to 0.44 wt %). These oxides appear to be mutually exclusive, with elevated Na_2O where there is depleted K_2O and visa versa. These patterns are repeated in a number of other elements, suggesting that the elements are coupled with either Na_2O or K_2O in certain minerals. Fe_2O_3 and MgO mimic the Na_2O pattern. These are most abundant in the sample from 160 m and least abundant in the sample from 65 m. In contrast, K_2O is least abundant in the sample from 160 m, a pattern repeated by Ba, Sr and to a lesser extent Cr. The top of the quartz-bearing mudstone, closest to the host sequence (250 m), is elevated in SiO_2, TiO_2, MgO, Na_2O, Pb, Nb, Zr, Y, La and Ce but depleted in K_2O, V, Cr, Ni, Ba and Sr compared with the rest of the quartz-bearing mudstone.

Quartz sandstone and mudstone at the top of the footwall display the highest Zr levels, while the upper mudstone (274 m) contains the most Mo and abundant V, but has lower La and Ce compared with the other lithologies. The basal rhyolite is low in SiO_2, TiO_2, K_2O, Ba and Cr, elevated in Al_2O_3, Fe_2O_3, MnO, MgO, Na_2O, Sr and V abundance and displays the highest levels of P_2O_5 (0.6 wt%) in the drillhole (Fig. 7.14). Alteration affected the late mafic dyke, which displays element abundances intermediate between the main part of the quartz-bearing mudstone facies and the top of the unit.

Host Sequence

The AI varies through the host sequence, from close to 100 (DDH 3, 400 m) to the lowest AI calculated 14 (DDH 3, 360 m). The CCPI is less variable, and consistently greater than 90 in these rocks (Fig. 7.14).

Figure 7.14 Geochemistry of the footwall (DDH 16A), host sequence (one sample in DDH 16A and five in DDH 3) and hanging wall (DDH 3). The first plot is the Ishikawa Alteration Index (AI) and the second the Chlorite-Carbonate-Pyrite Index (CCPI). See text for definitions. The next ten plots are of the major element oxides (wt %) and the subsequent 11 plots are trace elements (ppm). Abundance scales vary from element to element. Lithological log is depicted on the left with a legend above and shows the main units in the footwall (quartz-bearing mudstone) and hanging wall (rhyolite). Sedimentary units are abundant in the upper footwall and the host sequence. A rhyolite is also present at the base of the footwall.

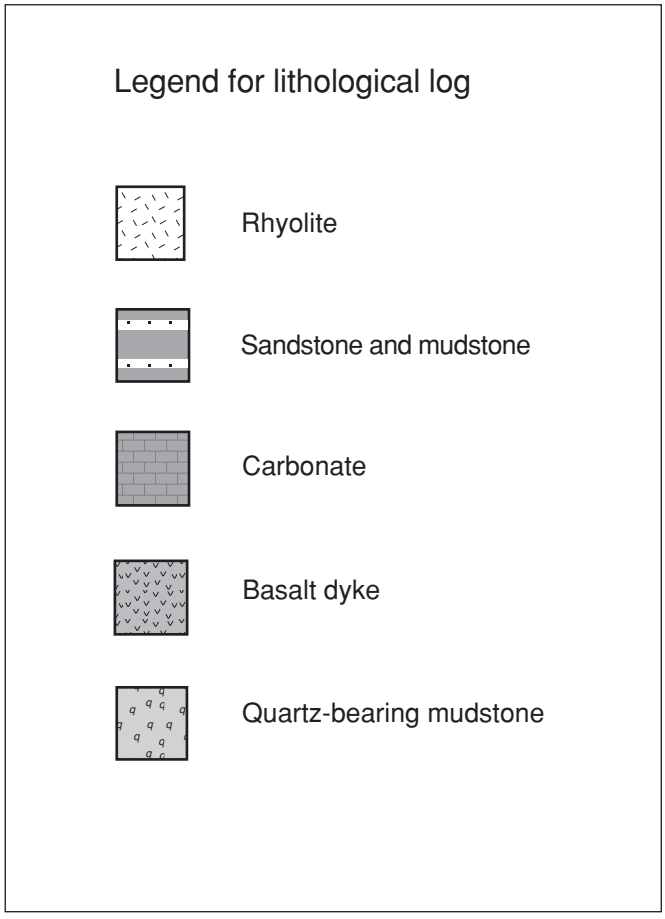

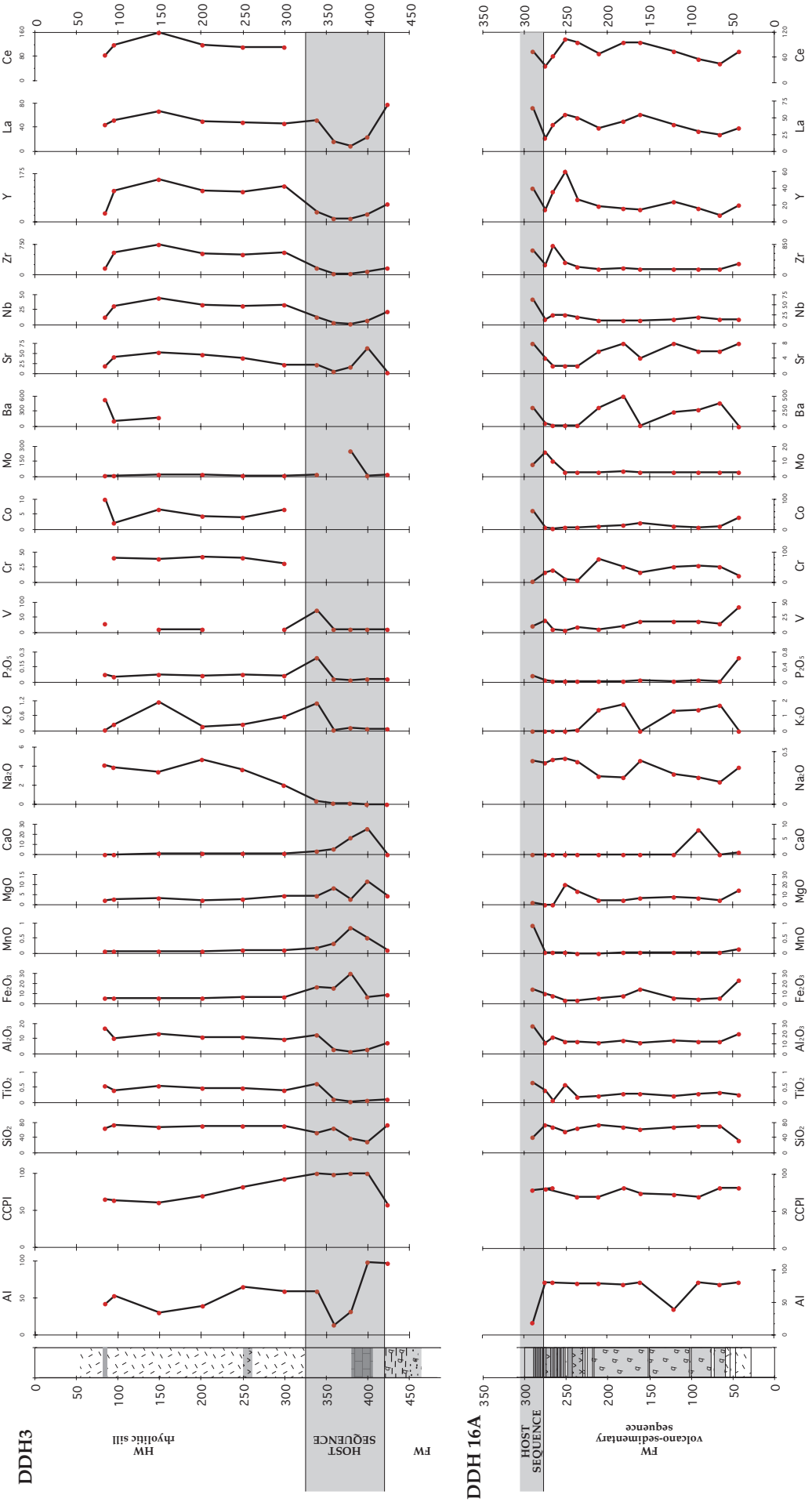
DDH3
HW
rhyolitic sill
HOST
SEQUENCE
FW
DDH 16A
HOST
SEQUENCE
FW
volcano-sedimentary
sequence
Al
CCPI
SiO2
TiO2
Al2O3
Fe2O3
MnO
MgO
CaO
Na2O
K2O
P2O5
V
Cr
Co
Mo
Ba
Sr
Nb
Zr
Y
La
Ce

The deepest sample from DDH 16 A is a talc and white mica schist, which is within the host sequence. This sample displays the highest levels of Co and MnO in DDH 16A and also has elevated TiO_2, Al_2O_3, Fe_2O_3, Na_2O, P_2O_5, Ba, Sr, Nb, and La and depleted values of SiO_2, K_2O, V, with the lowest value of Cr (4 ppm) for DDH 16A.

The host sequence was also sampled between 328 and 415 m in DDH 3. Although lithology does control some variations in the geochemistry of the host sequence, such as the variable SiO_2 and CaO, there is still an overall low abundance of TiO_2, Al_2O_3, Na_2O and K_2O. Variations in Fe_2O_3, MgO and MnO content are apparent even within carbonate (Fig. 7.14). Overall the host sequence displays erratic Mo and Cr values, has low Ba and HFSE (Nb, Zr, Y, La and Ce) and high V and Sr (Fig. 7.14).

Hanging wall

The hanging wall in DDH 3 is dominated by a rhyolitic sill (96–300 m) with a mudstone at 85 m and a volcaniclastic unit at 250 m. The AI is above 50 near the host sequence, decreasing to 31, 150 m from the contact and increasing to near 50 in the uppermost samples. The CCPI begins above 90 near the host sequence and reduces steadily to 64 with distance from the host sequence (Fig. 7.14).

The hanging wall displays flat abundance patterns for most oxides (Fig. 7.14). The exceptions are Na_2O and K_2O, which are almost mutually opposed. Na_2O increases away from the host sequence to 200 m, where it is most abundant before decreasing again slightly at 150 m. In contrast, K_2O is most abundant at 150 m, at its lowest level at 200 m and more abundant towards the host sequence. The patterns of the LILE and HFSE (Sr, Nb, Zr, Y, La, Ce) all display curves with maximum elemental abundances in the sample from 150 m (Fig. 7.14). Although metal data sets for the hanging wall are incomplete, most display little variation with low overall elemental abundances (Fig. 7.14).

7.4.4 DISCUSSION

From the geochemistry, it is apparent that overall the sequence through the footwall and into the host is low in Na_2O (<0.5%). It is only more abundant in the upper portions of the hanging wall (<5%), furthest from the host sequence. Accompanying low Na is a marked increase in MgO, MnO, Fe_2O_3, and CaO near and through the host sequence. K_2O is also low (<1.8 wt%), but more abundant overall than Na_2O. These two oxides appear to be immiscible. Carbonate alteration is discussed in detail in Chapter 8. Quartz-dominated zones are patchy, but are not apparent in the compositions. Abundant quartz is present near the top of the footwall, between the carbonate lenses and above the upper carbonate lens. Quartz deposition is favoured in units with a high surface area, where silica can readily nucleate (Rimstidt & Barnes 1980). Pre-existing quartz in volcaniclastic units and fine-grained sedimentary units within the host are ideal locations for silica precipitation.

Low Na in the Footwall and Host Sequence

Albite is absent in the footwall and host sequence, but present in the hanging wall rhyolite. The low abundance of Na in these sequences is confirmed by the geochemistry. Na is depleted in the

footwall of many VHMS style deposits (Large 1992, Large et al. 2001*)*. This depletion is caused by the breakdown of feldspars or glass. At Onedin, the footwall is dominated by quartz, chlorite and white mica, so minor Na detected is probably housed in sodic white mica. Reflectance analyses by SWIR on samples from drillhole DDH 16A support this hypothesis. Paragonite is indicated where infrared spectra display an absorption trough at wavelengths of 2192–2196 nM (Fig. 7.13) (Pontual et al. 1997). White mica is either paragonite where Na is present in the A-site, or muscovite where K fills this site, although sodic muscovite can accommodate Na in up to 20% of the A-sites. The contrasting patterns in abundance of these oxides may reflect the miscibility gap between muscovite and paragonite (Spear 1993). Furthermore, the mimetic pattern of Ba and Sr with K can be explained by the large interlayer site in muscovite, which can accommodate large ions such as Ba and Sr. The interlayer site is much smaller in paragonite. Consequently, the large ions are excluded where Na is abundant (Deer et al. 1992). The abundance of Fe and Mg coupled to Na, suggests that low muscovite samples have more abundant chlorite.

New spectral analyses tools such as Portable infra-red Spectral Analyser (PIMA) allow the identification of white mica composition and crystallinity (Pontual et al. 1997, Thompson et al. 1999). From these studies sodic white mica has been identified in hydrothermal systems and reported close to ore in a number of VHMS deposits, including the Rosebery hanging wall, highly altered portions of the Tharsis deposit and the proximal zones of Highway-Reward (Herrmann et al. 2001). A sodic muscovite signature can also be seen in the spectra from samples of KPD 35 (wavelength 2196–2199, Fig. 7.13), another drillhole through the footwall and directly under a sulfide zone. No shift is registered in the white mica compositions. No drillholes penetrate the footwall further from the sulfide zone. In the absence of further data, it is uncertain if the presence of the low AlOH-adsorption white mica, can be used as a vector to ore at Onedin.

Abundant Mg in the host sequence

Abundant Mg is evident in gangue minerals associated with sulfide minerals in the host sequence. Talc forms a major gangue mineral and is also common in the upper footwall below the sulfide zones. Dolomite and Fe-dolomite are the main carbonate gangue minerals and host sulfide minerals. Chlorite in the host sequence contains more Mg than chlorite in the footwall (Fig. 7.11A).

Alteration Indices

With the exception of the sample from DDH 16A 120 m, the AI is high throughout the footwall and variable in the host rocks and hanging wall. Reduction in AI in the host sequence is related to the abundance of calcium in dolomite and tremolite.

The CCPI is high throughout the footwall and host, and reduces gradually in the hanging wall away from the host rocks. The overall high CCPI indicates that chlorite is abundant in these rocks. The trend to lower CCPI values maps a change to less chlorite and more albite in the hanging wall with distance from the host sequence (Fig. 7.14). This pattern in the CCPI suggests that all these rocks underwent alteration, with a decrease in alteration intensity in the hanging wall away from the host sequence.

Box plots of AI against CCPI (Large et al. 2001, 2002) for the Onedin sequence and for other rhyolite and rhyodacite in the area, indicates that the hanging wall at Onedin is definitely altered

compared with the least altered samples from Koongie Park (Fig. 7.15). Most of the samples plot as a scatter outside the least altered modern arc volcanic box. Chlorite and carbonate in many of the samples indicate that they have undergone alteration and have probably shifted up the chlorite/carbonate/pyrite (CCPI) axes from their original values. Samples are depleted in Na_2O and K_2O and enriched in MgO relative to least altered samples.

A-type granite and rhyolite are thought to be comparable to the KPF rhyolite (Chapter 6). A-type suites plotted on the AI versus CCPI box plot fall within the field of least altered, modern arc, rhyolite (Fig. 7.15), although some from the Lachlan Fold Belt (Collins et al. 1982) plot near or below the bottom of the box. This pattern reflects low iron and magnesium relative to sodium and potassium in A-type suites. Only one sample from the Koongie Park area plots within the least altered box for modern arc rhyolite. This is from Sandiego. The sample displaying a low alteration index contains albite. Even the sample most likely to be closest to the precursor felsic volcanic, from SND 2 150.1 is elevated in CCPI relative to A-type suites. The least altered sample has a CCPI and AI about 20% lower than most of the Onedin A-type rhyolite.

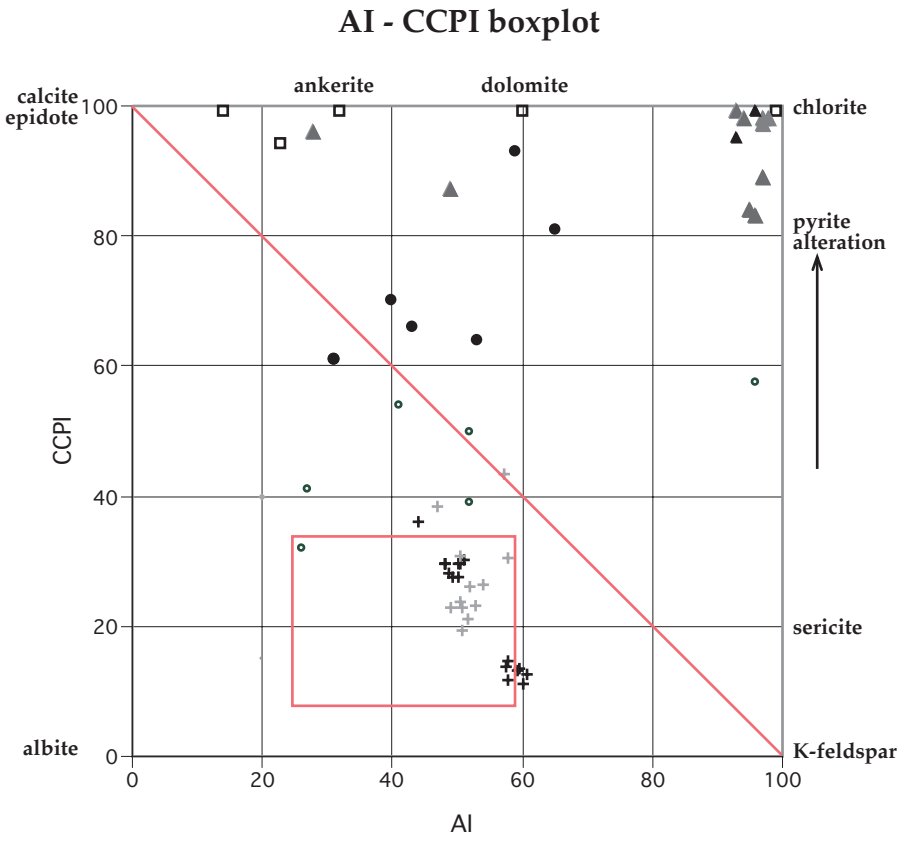

Figure 7.15 Boxplot of AI against CCPI showing the footwall (triangles), host (squares) and hanging wall (solid circles) at Onedin. All these plot in the hydrothermal alteration field above the calcite-feldspar line. The crosses depict typical A-type felsic rocks (Collins et al. 1982, Eby 1990), which fall within or below the least altered field for modern arc rhyolite (Large et al. 2001, Gifkins et al. in press). Least altered samples of felsic volcanics from Sandiego (small open circles) fall in this field, demonstrating the alteration in the hanging wall at Onedin which have a higher CCPI. Most alteration appears to be related to chlorite and chlorite-pyrite from this plot with abundant chlorite and carbonate in the host sequence.

Most of the alteration halo is chlorite or carbonate related. The box plot does not detect quartz alteration, which is also apparent throughout the sequence.

7.4.5 CONCLUSION

Elevated alteration indices indicate that the footwall, host and hanging wall at Onedin were intensely altered. The footwall and host sequence contains a semi-conformable, low-Na zone, which is less developed in the hanging wall. Mg-enrichment in the host sequence, close to massive sulfide, is similar to alteration haloes in many VHMS deposits of different ages worldwide (Franklin et al. 1981, Urabe et al. 1983, Large 1992). The asymmetry of the effect of alteration in the footwall and hanging wall indicate that there was a directional component to the alteration with higher intensities beneath sulfide deposits. The presence of hanging wall albite and quartz overprinted by phyllosilicates, as well as disseminated zinc in DDH 5 (Fig. 7.1D), indicates that the hydrothermal system continued circulation after emplacement of the hanging wall sill. Such a setting places the hydrothermal cell beneath the seafloor.

7.5 ISOTOPE GEOCHEMISTRY

7.5.1 PB ISOTOPES

Pb isotopes were applied to the Koongie Park prospects by Gulson et al. (1982) and Gulson (1986) as part of an Australia-wide study by CSIRO to examine base metal ore bodies in different mineralised districts. Pb isotope values from gossan were compared to the underlying sulfide Pb isotope signatures. More data was collected on Onedin (Dean 1992, 1993 and Gemmell reported here, Appendix 9). All the ore bodies display near identical Pb isotope values (Fig. 7.16), although some have a more radiogenic signature than others. Onedin has the least radiogenic signature. The Pb isotope results indicate a common Pb source region. The similarity of the Pb isotope values led Dean (1993) to suggest that all the KPP formed from the same hydrothermal fluid.

Age calculations from the Pb isotopes of galena, indicate that these sulfide minerals formed 1830±90 Ma ago (Gulson, 1986) or around 1825 (Dean, 1992, 1993). Both results are consistent with the zircon ages for deposition of the KPF (1843 ± 2) (Page et al. 1994) and deformation and metamorphism of the Halls Creek Orogeny, constrained by the post-tectonic intrusion of the Loadstone Monzogranite around 1827± 3 (Blake et al. 1999).

All the data from Onedin plot above the Stacey and Kramers (1975) curve on a $^{206}Pb/^{204}Pb$ versus $^{207}Pb/^{204}Pb$ diagram (Fig. 7.16), suggesting input of a radiogenic Pb source. A radiogenic Pb isotope signature is typical of the Pb isotope values from all base metal deposits throughout the Halls Creek Orogen (Nelson 1999). The elevated $^{207}Pb/^{204}Pb$ values suggest that the galena in these base metal occurrences were derived from source areas with higher U/Pb than the Earth's mantle, or model ore growth curve reservoirs. More work is required to develop a Pb isotope model for this area. Measurements of Pb, and the Pb isotopic values of minerals such as biotite and feldspar, in typical rocks of the Hall Creek Orogen, is required to provide the background for any meaningful Pb source modelling.

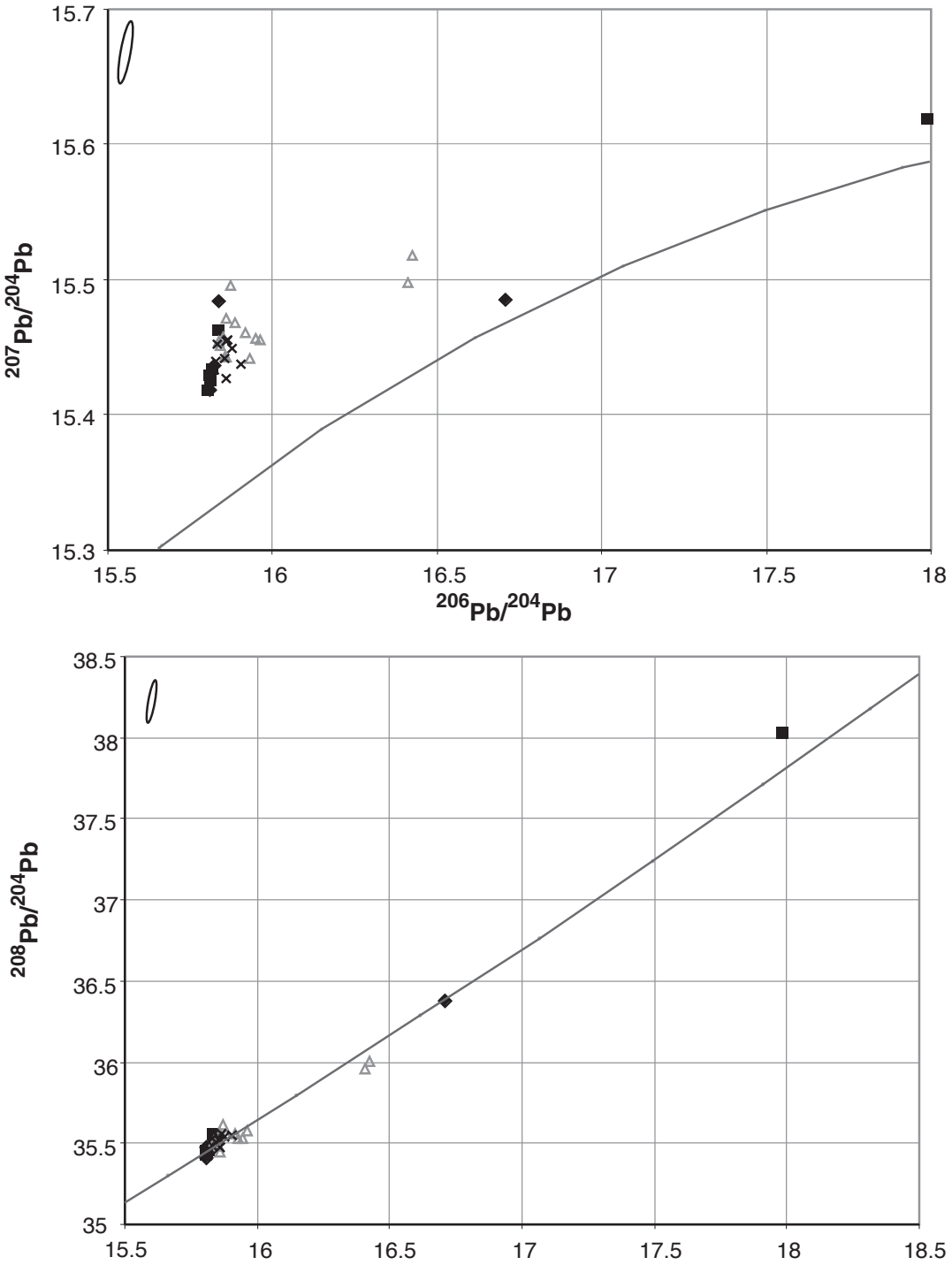

Figure 7.16 Pb isotopes plots for the Koongie Park prospects, including Onedin data obtained by Dean (1992 and 1993, solid diamonds), Onedin data obtained by B. Gemmell in 1992 (unpublished, solid squares) and data for Sandiego (open triangles) and Gosford (crosses) gathered by Gulson et al. (1982). All data are plotted against the Stacey & Kramers (1975) growth curves. The Pb isotopes at the prospects are overlapping. The data plotting with higher $^{206}Pb/^{204}Pb$ could be the result of radiogenic addition or caused by experimental errors (Dean 1993). Most data plot above the Pb growth curve, indicating a more radiogenic source for the Pb in these rocks and minerals. Error ellipses in the upper left corner of each diagram.

7.5.2 SULFUR ISOTOPES

Sulfur isotopes were analysed using the laser probe technique (Huston et al. 1995b), with only two samples using conventional mass spectrometry. Sphalerite, pyrite, chalcopyrite and pyrrhotite were tested (Fig 7.17, Appendix 9). All sulfide minerals tested have $\delta^{34}S$ values between –1 and 7‰ with an average of +3.0‰. This tight cluster (standard deviation of 1.8) of results may indicate a homogenous sulfur source. Similar results are found in other Palaeoproterozoic deposits e.g., Arizona (Eastoe et al. 1990).

Seawater sulfate values have varied over time and are tracked by curves as far back as the Neoproterozoic (Claypool et al. 1980). Although estimates for Palaeoproterozoic and Archaean oceans are available (Canfield 1998, Canfield & Raiwell 1999), these are based on scattered information. Best estimates for seawater sulfate values in the Palaeoproterozoic are $\delta^{34}S$ =10–18‰ (Strauss 1993, Strauss & Beukes 1996). If seawater was drawn into the hydrothermal system, and heated to 250°–400°C, this would cause an 18‰ shift (Ohmoto & Rye 1979) in $\delta^{34}S$ values to between –10 and 0‰. Magmatic sulfur has $\delta^{34}S$ values close to unity (0‰). Biogenic, sedimentary sulfide formed during the Palaeoproterozoic have $\delta^{34}S$ values between –30‰ and 20‰ (Strauss & Beukes 1996). The similarity of the S isotope values for the three main sulfur sources impedes identification, or modelling, of the sulfur sources for Palaeoproterozoic deposits.

Temperature estimates on pairs of sulfide minerals within samples gave no meaningful results (Appendix 9). The lack of useful results suggests that the mineral assemblages are not in equilibrium with respect to S isotopes. Metamorphic changes of pyrrhotite to pyrite, as well as low sulfur fugacity, may help explain the inconsistent results. Low S fugacity prevents the equilibration of S isotopes (Ohmoto & Rye 1979) and is also evident from abundant pyrrhotite and patchy magnetite.

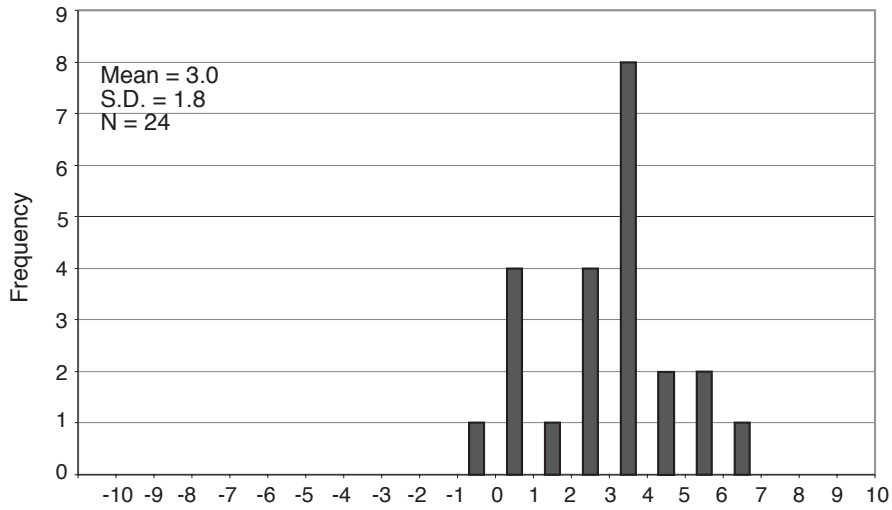

Figure 7.17 Distribution of sulfur isotope values obtained from pyrite, pyrrhotite, sphalerite, galena and chalcopyrite from Onedin. The $\delta^{34}S_{CDT}$ values range from –1‰ to 7‰ average 3‰ and have a standard deviation of 1.8.

7.6 EVIDENCE FOR VHMS ORIGIN?

Although the volcano-sedimentary setting of Onedin is appropriate for a VHMS deposit (Chapter 4) it is also appropriate for skarn deposits (Ashley & Wilmott 1997). Furthermore, overprinting by deformation and metamorphism controls many of morphological features of the sulfide zones and obscures their origins. Despite this, some features indicate that the massive sulfide at Onedin formed soon after deposition or diagenesis, possibly related to the influx of silicic magma.

The overall patterns of alteration and composition of the footwall, host sequence and hanging wall are important evidence for the origin of sulfide zones at Onedin. Low Na in the footwall, Na present in the hanging wall and abundant Mg in the host sequence are consistent with alteration haloes documented in many VHMS deposits (Franklin et al. 1981, Large 1992). The broad area of altered rock, especially in the footwall and extending into the hanging wall, indicates that these units reacted with large amounts of fluids. These fluids were not restricted to veins, fractures or cleavage, as would be anticipated in a deformation-related deposit and alteration was not restricted to the carbonate and adjacent areas, as in skarn deposits. The alteration pattern also provides evidence against a skarn origin for the sulfide zones. Zinc skarns display well developed zonation patterns of garnet-clinopyroxene, epidote-amphibole and quartz-magnetite. Most are Mn rich (Einaudi et al. 1981, Meinert 1992, 1997, Ashley & Willmott 1997). These minerals are rare or absent at Onedin, which is almost devoid of Mn. At Onedin, quartz-magnetite is usually part of ironstone and disseminated in the surrounding sedimentary sequences, but generally absent from carbonate. Only an isolated occurrence of magnetite + andradite occurs at the northern edge of the deposit in DDH 3 (382 m). An alteration halo in the hanging wall also indicates that this unit was present at the time the hydrothermal fluids were circulating through the succession.

Although totally recrystallised, and portions remobilised, rare primary features are evident in sulfide minerals away from the massive sulfide bodies. Disseminated and veined pyrite associated with galena and sphalerite are present in the deeper portions of the carbonate-hosted ore lenses (KPD 36, 408m). Some remnant pyrite textures, consistent with botryoidal growth of pyrite/pyrrhotite within carbonate are present in the top of the upper carbonate-hosted sulfide zone (Fig. 7.4). These textures may have developed early.

Further evidence for pre-deformation alteration includes randomly oriented talc crystals, within recrystallised sphalerite patches (Fig. 7.7A) and carbonate paragenesis (Chapter 8).

Talc crystals formed during D_1 and D_2 are aligned with S_{KP1} and S_{KP2} cleavages. Random orientation of the talc crystals within massive sulfide lenses indicates that they formed in the absence of any stress regime and could pre- or post-date deformation. The sphalerite around the talc is recrystallised and the talc crystals themselves are strongly kinked, suggesting that they underwent deformation after they grew (Fig. 7.6A). Crenulated talc and carbonate, devoid of cross-cutting crystals, near the sphalerite indicate that the talc grew prior to deformation.

Carbonate preserves glass bubble-wall structures (Chapter 8), indicating that some of the carbonate is secondary and replacing volcanic units. Carbonate replacing rhyolite is reported from the Thalanga VHMS deposit (Herrmann 1994, Hill 1996, Herrmann & Hill 2001). Cathodo-luminecsence reveals that sulfide minerals are related to an iron-rich carbonate, which pre-dates metamorphic calcite. To explain this observation a large amount of Fe-bearing fluid entered the

sequence prior to metamorphism and deformation. Furthermore, carbonate textures (Chapter 8) are the same as textures developed in some other carbonate associated VHMS deposits (Orth & Hill 1994, Allen 1997, Herrmann & Hill 2001).

Sulfide veins cross-cuts deformation features. The veins are only a minor component of the sulfide zones. The veins may be related to fluid-assisted remobililation (Marshall et al. 2000) associated with peak metamorphic conditions, which post-date D_1 and D_2, or later deformation events (D_3 or D_4, Chapter 3).

A sub-seafloor replacement VHMS model explains the asymmetry of the alteration pattern at Onedin and alteration of the hanging wall. It explains the destruction of feldspar in the footwall and is consistent with the retention of Na in albite in the hanging wall (Urable et al. 1983). It also explains the addition of Mg, Si and Ca in the host sequence. Alteration of calcareous mudstone, mudstone and glassy sediments to carbonate was probably related to the same system. Pre-metamorphic growth of the talc crystals associated with the sphalerite in the sulfide zones, is consistent with this model. Although metamorphic recrystallisation and remobilisation has changed the appearance of the sulfide zones, these processes are unlikely to have caused large scale transport of sulfide minerals. Gilligan & Marshall (1987) and Marshall et al. (2000) suggested that remobilisation processes only move sulfides over tens of metres with larger mass transfers improbable. It is most probable that sulfide mineralisation was already present at Onedin when deformation and metamorphism affected the KPF.

7.7 COMPARISON WITH OTHER VHMS DEPOSITS

7.7.1 THREE DIMENSIONAL ARCHITECTURE OF SOME MODERN VHMS DEPOSITS.

Although submarine hydrothermal systems have been studied over the past 35 years, since the discovery of activity in the Red Sea (Miller et al. 1966) and later near the Galapagos Islands (Corliss et al. 1979), knowledge has been largely restricted to near surface sampling. Drilling during the last 10 years has revealed the third dimension of submarine hydrothermal activity. Drill studies of the internal and sub-seafloor architecture of accumulating VHMS deposits provide the only modern analogues of ancient sub-seafloor deposits such as Onedin.

Drilling commenced at the sediment-hosted Middle Valley deposits on the Juan de Fuca Ridge, off the NW coast of North America in 1991 (ODP Leg 139) (Davis et al. 1992) and was followed up in 1996 (ODP Leg 169) (Zierenberg et al. 1998). The TAG hydrothermal mound on the Mid-Atlantic ocean ridge was drilled in 1994 (ODP Leg 158) (Humphris et al. 1995, Herzig et al. 1998, Petersen et al. 2000). Most recent drilling targeted PACMANUS hydrothermal field, on the crest of an andesite-dacite-rhyodacite ridge overlying older rifted arc crust in a backarc basin late in 2000 (ODP Leg 193) (Binns et al. 2001). These three active seafloor hydrothermal systems vary greatly in their sub-seafloor architecture.

Middle Valley hydrothermal field includes two main deposits called Bent Hill and ODP, which exhibit mounds of clastic massive sulfide on the seafloor and sub-seafloor massive sulfide lenses extending down into feeder zones to about 220 m below seafloor (bsf) (Davis et al. 1992, Zierenberg et al. 1998). An estimated 15–20 Mt of massive sulfide is contained in these deposits

(Goodfellow et al. 1999). Surrounding the massive sulfide deposits are altered sediments with chimneys at the seafloor composed of anhydrite and barite with sulfide minerals. The lowermost portion of the deposits is marked by deep copper zones which contain Cu- and Fe-sulfide minerals replacing altered sandy turbidites.

TAG is on a sediment-free ridge and is mainly composed of breccias. These breccias commence with chloritised root zones in the underlying basalt and form an overlying 200 m diameter by 50 m high mound. The main mound-building mineral is anhydrite, with less abundant silica and pyrite and the outer carapace composed of Fe-oxyhydroxide, chert, sphalerite and pyrite (Humphris et al. 1995, Petersen et al. 2000). Most of the massive sulfide minerals are found on the outer portions of the mound, because the inner portions have undergone an extended history of zone refining (Petersen et al. 2000).

Drilling of the active felsic-hosted hydrothermal system at PACMANUS in the Manus Basin north of Papua New Guinea was completed late in 2000 and only a preliminary report on findings is currently available (Binns et al. 2001). Despite poor core recovery (<10%) this drilling (to 387 m bsf) revealed fresh rhyodacite to dacite overlying highly altered and sulfide mineralised lavas. Alteration minerals include silica, chlorite+smectite and chlorite+illite, clays, pyrophyllite and variable amounts of pyrite and anhydrite. Quartz + chlorite dominate in the deeper zones. These zones were cross-cut by anhydrite+pyrite+quartz veins. Pyrite is the dominant sulfide mineral, with only minor chalcopyrite, pyrrhotite, accessory sphalerite and rare marcasite, galena and tennantite. Zones of pyrite enrichment are coincident with abundant magnetite in vein halos.

From this summary, it is apparent that the dominant sulfide minerals vary temporally within the sub-seafloor systems, which can be dominated by sulfide breccias, veins or lenses. The mound at TAG is mainly above the seafloor and composed of anhydrite, deposited from heated seawater. At Middle Valley and PACMANUS some clastic sulfide minerals and sulfide mounds are present above the seafloor, but more abundant sulfide minerals occur beneath the seafloor in hydrothermally altered sediments and volcanics. Various silica polymorphs, anhydrite, chlorite, smectite, illite, muscovite, albite and calcite are the main alteration minerals. Wairakite and epidote occur in high temperature upflow areas in Middle Valley (Goodfellow & Peter 1994). The main ore lenses at Middle Valley are composed of pyrrhotite, sphalerite, isocubanite and chalcopyrite. One zinc-rich lens was intersected at 'ODP' deposit. Pyrite is the main sulfide mineral at PACMANUS and TAG, although TAG also has zinc-rich areas on the outer carapace.

Although none of these modern examples closely resemble Onedin, Middle Valley has some similarities. The sub-seafloor parts of the Middle Valley deposits, with sulfide minerals hosted in turbidites is similar to parts of the chlorite schist-hosted sulfide zones at Onedin. Carbonate is present at Middle Valley, albeit at low abundances, distal to the massive sulfide, whereas carbonate at Onedin forms the main host to high grade base metals.

7.7.2 ANCIENT SUB-SEAFLOOR DEPOSITS

Ancient sub-seafloor deposits provide a more complete picture of the range and diversity in three dimensions of VHMS deposits. Recent studies include descriptions of the Archaean Kidd Creek deposits in the Timmins district (Barrie et al. 1999), the Ansil deposit from the Rouyn-Noranda district (Galley et al. 1995) and Chisel Lake deposits in the Palaeoproterozoic Churchill Province (Galley et al. 1993) of Canada. Several deposits of Palaeoproterozoic age in Sweden, including

Renström in the Skellefte district and Garpenberg in the Bergslagen district, have recently been interpreted as sub-seafloor deposits (Allen et al. 1996a, b). In Australia, Highway-Reward (Doyle & Huston 1999) and West Thalanga (Hill 1996, Herrmann & Hill 2001) in the Cambro-Ordovician Mt Windsor Subprovince, at least some of the ore lenses at Rosebery (Allen 1994) in the Cambrian Mt Read Volcanics, as well as the Silurian Currawong deposit in northeastern Victoria (Bodon & Valenta 1995) are all considered to be sub-seafloor VHMS deposits. Features of well described examples from this literature are summarised in Table 7.4 .

The deposit at Onedin has a stratabound, lens-like morphology, similar to Rosebery, Chisel Lake, North Chisel, Kidd Creek, West Thalanga and the outer parts of Ansil (Table 7.4). In chlorite schist, massive sulfide minerals and abundant quartz and chlorite characteristically occur in permeable units. Mineralisation and alteration were focused in permeable units at other sub-seafloor deposits, including sandy beds in turbidites, e.g., Currawong and the hanging wall at Ansil, pumice breccia, e.g., Rosebery and volcaniclastic units, e.g., West Thalanga. At Onedin fluids also entered reactive units. Although carbonate is associated with massive sulfide deposits at West Thalanga, Rosebery and Hercules (Khin Zaw & Large 1992), replacement of carbonate is only documented at Chisel Lake and North Chisel Lake (Table 7.4).

7.8 GENESIS OF THE SULFIDE ZONES AT ONEDIN.

Massive sulfide deposits at Onedin formed when a metal-bearing fluid interacted with carbonate. Carbonate is present as pods within the Onedin Member between Onedin South and Rockhole, and associated with other prospects, such as Onedin and Gosford. It is uncommon away from these areas (Chapter 8). Only two carbonate units, mapped 100 and 200 m above the Onedin Member near Rockhole, occur as thin (2 m thick x 300 m) turbidites (Chapter 4). Volcanic detritus comprises the sand sized-component with carbonate mudstone. Carbonate-bearing turbidites are different from the complex carbonate at Onedin. Although a succession of carbonate mud and glassy sediment is a likely precursor to the Onedin carbonate lenses, much of the carbonate was probably deposited during hydrothermal alteration (Chapter 8). Carbonate was subsequently replaced by metal-bearing fluids, in a sub-seafloor setting. Paragenesis of the sulfide minerals cannot be constrained as they are annealed. It is assumed that all the sulfide minerals deposited together.

The Onedin sulfide zones formed within a submarine, synvolcanic sequence. At the onset of significant hydrothermal activity the seafloor area was composed of 100–200 m thick porous volcaniclastic units overlain by fine-grained wet sediments. Chemical and suspension sedimentation ensued allowing the accumulation of chert, ironstone and muds (Chapter 4).

Intensification of local hydrothermal activity in the Onedin area probably accompanied the intrusion of the sill complex, which form the hanging wall at Onedin (Chapter 9). Increased local heat flow and movement of fluids through the porous sequences, caused alteration of the sediments, resulting in a low-Na volcaniclastic footwall and abundant Ca, Mg, Si in the host sequence. Circulating fluids were trapped by low porosity, wet muds and the overlying sills and associated, locally lithified intruded sediments. Carbonate deposited in calcareous muds and glassy

Table 7.4 Summary information on the characteristics of some ancient sub-seafloor VHMS deposits. Deposits listed in order of age: Archaean to Phanerozoic.

Deposit Location. Age. Tonnage.	Deformation and Metamorphism.	Morphology.	Rocks and Alteration style. Footwall.	Host.	Hanging wall.	Ore bodies.	Ore minerals.	Sub-seafloor characteristics.	Genesis.	References.
Kidd Creek Timmins Ontario, Canada. Archaean (2716±0.6 - 2715±1.2 Ma). 138Mt @2.4% Cu, 6.5% Zn, 0.23% Pb, 90g/t Ag 0.15% Sn.	Folded by F1 and smaller F2 folds; lower-middle greenschist facies metamorphism.	Tabular, stratiform ms lenses, several kms long, 250-500 m wide, 20-50 m thick.	Mafic-ultramafic rocks in the FW. Semi-conformable qtz+ser.	Felsic volcanic rocks: rhyolite dome, breccias, with some mudstone. Fe-rich chlorite close to mineralisation, Mg-rich halo, sid, qtz, tm.		3 main ore bodies: North, (NOB) Central (COB) and South (SOB). Within these are 3 main ore types which can be further subdivided: C-type = massive banded sph- rich ore; A-ore = Cu-rich and related stringers; breccia ore = sulfide clast-rich ore.	Sph, py, po (more common in the deeper portions of the ore bodies), cpy (also more common in the deeper portions of the ore body), ga, Ag-rich minerals (such as tet; Ag-py). Co-Fe-As sulfides, cas and st.	Remnant silicified rhyolite in ms; gradational contact between ms & unmineralised fragmental rocks; replacement fronts in HW; lack of exhalites; stratiform alteration zones and cpy stringer areas.	Formed in a graben near a main fault during volcaniclastic deposition. Much of the deposit is sub-seafloor between 50-100 m. Buried during formation as some of the NOB sulfide clasts are found in breccia in the FW of SOB.	Barrie et al. 1999.
Ansil Rouyun-Noranda, Canada. Archaean. 1.58 Mt @ 7.2 % Cu, 0.9 % Zn, 26.5 g/t Ag, 1.6 g/t Au	Essentially undeformed. Lower greenschist facies metamorphism except in the aamphibolite-grade contact aureole with the Lac Dufault pluton.	Lens-like body, 320 m x 150 m x 6 m thick, but can be up to 35 m thick.	Underlying rhyolite is Na depleted. Alteration was focussed along long-lived faults. Early HT breccias infilled by qtz+alb+sp+py and wall rock altered to ser+qtz+sph+py, overprinted by chl. Later calc-silicate alteration and mgt vein stockwork accompanied by ep+alb+chl alteration.	Quartz-porphyry, finely-layered tuff. Chl associated with po+cpy overprinting Single beds have silicified tops with sulfide minerals infilling coarser bases.	Extends over 500 m through the Rusty Ridge Formation of andesitic hyaloclastites and lavas. The hyaloclastites are selectively altered, often with lenses of po+cpy+chl, which grade outwards to sph+po+ser.	One ore body, with stringers extending below the ms lens and lenses of cpy-py and mgt in the hanging wall.	Ore minerals are sph, po, py, cpy, mgt.	Overprinting of various stages of alteration and mineralisation Alteration and mineralisation into the HW. Large Na-depletion HT cell.	3 stages of formation: 1) Associated with Na depletion, HT breccia formation and deposition of breccia infill, ser+qtz +sph+py alteration in FW and py+sph in the host tuffs; 2) Cu-rich overprinting, forming po+cpy stringer and chl +qtz alteration in the FW, cpy+po and chl deposition in the tuff and lenses of cpy+po+chl to sph+po+ser in HW; and 3) Calc-silicate and Ca-Fe skarn below and in contact with ms, FW mgt stockwork and ep+alb+chl alteration, dissem. mgt in the base and as a lens and disseminated in the HW.	Galley et al. 1995.

Table 7.4 cont.

Deposit Location. Age. Tonnage.	Deformation and Metamorphism.	Morphology.	Rocks and Alteration style. Footwall.	Host.	Hanging wall.	Ore bodies.	Ore minerals.	Sub-seafloor characteristics.	Genesis.	References.
Chisel Lake (CL) and North Chisel Lake (NCL) Flin Flon Belt, Canada. Palaeoproterzoic. CL: 3.57Mt @ 0.42 % Cu, 11% Zn, 56.3 g/t Ag, 2.17 g/t Au. NCL: 2.58 Mt @ 0.22 % Cu, 8.9 % Zn, 0.4 % Pb, 23.3 g/t Ag, 0.5 g/t Au.	Undergone 3 deformation events and lower amphibolite facies metamorphism.	Series of 9 folded, elongate, stratiform massive to semi-massive sulfide lenses underlain by discordant zones of disseminated and vein sulfide. CL < 40 m thick, NCL < 20 m thick	Footwall alteration occur in a dacite. Semi-conformable, keel-shape. Outer bio+gar zone: qtz+bio+mus+plag+cal+ep+ga) ch+stau zone: qtz+Mg-bio+mus+ga+Mg-ch, stau, patches near the top of the FW of ser+kyan zone: qtz+Mg-bio+mus+Mg-ch+kyan. Discordant, pipe-like siliceous stringer zones (qtz+Mg-bio+mus+gah) and an amphibole stringer zone (qtz+Mg-bio+plag+Mg-ch+gah+hb+t).	CL: coarse dolomite lenses and patches between the ore. Carbonate content increases upwards. Carbonate associated with tremolite skarn at base of sulfide deposits. NL: silicate-dolomite layers between the sulfide minerals. Matrix of ch+Mg-bio+ser+Mn-ga+cor+kyan+and+stau+gah.. Also Mg-bio+trem+mic.	CL: mafic turbidite wackes no alteration, but heterolithic breccias at the northern end are amp+qtz+ga or qtz+bio+po, Upseqeunce, patchy silicification in basalt.	Cu-Fe-rich bases, Zn-Fe-Pb-rich tops. Thick CL ores: crudely interlayered sph+py and sph and minor minerals and tellurides with layers of py. Skarn zones contain apy>ga>sph>cpy>po>bn>>jordanite, ten, el, Au. NCL: py and sph dominant sulfide minerals, massive po near HW.	Py, sph main sulfide minerals. Minor minerals include cpy, po, ga and apy. Trace sulfide minerals:jordanite, bournonite, boulangerite, meneghinite, ten, tet, gudmundite, hessite, Bi_2Te, altaite, el, Au, Ag, Bi, As.	Skarn development phase of the ore body. Associated with Cu-Fe minerals and chlorite.	Metal zonation and HT alteration consistent with a VHMS deposits formed at and later below the seafloor. Focussed fluid flow through discordant-fault-related zones. Carbonate exhaled (?) onto the seafloor and was dolomitised by Mg-rich fluids associated with the ore-bearing fluids. Overprinting of early, lower T carbonate by higher T fluids to produce the trem and Mg-bio-mic skarn.	Galley et al. 1993.
Rosebery K Lens, western Tasmania, Australia, Cambrian. ?28.3 Mt @ 14.3 % Zn, 4.5 % Pb, 0.6 % Cu and 145g/t Ag, 2.4 g?t Au.	Two phases of Devonian deformation; greenschist facies metamorphism.	16 lenses which vary in size from 0.1 to 5 Mt. K-lens Lens-like body 400 m x 20-50 m.	Rhyolitic and dacitic pumice breccias, qtz+feld+bio porphyry sill. Alteration halo: outer , least altered albite-bearing zone,then the sericite zone, (ser+Mn-Fe cb+qtz+ch) then chlorite zone (ch±ser±cb+py) and at the same level quartz-sericite zone (qtz+ser+py).	Upper pumice breccias, porphyry sill, volcaniclastic sandstone and black shale. Alteration halo is chlorite zone (ch±ser±cb+py) and at the same level quartz-sericite zone (qtz+ser+py). With albite-bearing zone at the fringes.	Volcaniclastic rocks. Alteration: quartz-sericite zone (qtz+ser+py), semi-conformable spotty Mn-Fe carbonate zone (Mn-Fe cb+ser±chl+py) then outwards to the sericite zone, (ser+Mn-Fe cb+qtz+ch) and albite-bearing zone volcanic rocks above.	Massive sulfide lenses of Zn and Pb with disseminated sph lens in the HW volcaniclastic rocks. Cu less extensive in massive sulfide lens.	Sph, ga, py, cpy, tet, with less common apy and po.	Replacement of the pumice breccias by massive sulfide minerals.	Hydrothermal fluids permeated upwards through a porous footwall pumice-rich volcanic unit until the fluids encountered cool seawater. Fluid mixing caused precipitation of sulfide minerals.	Allen 1994, Large et al. 2001.

Table 7.4 cont.

Deposit Location. Age. Tonnage.	Deformation and Metamorphism.	Morphology.	Rocks and Alteration style. Footwall.	Host.	Hanging wall.	Ore bodies.	Ore minerals.	Sub-seafloor characteristics.	Genesis.	References.
Highway-Reward, Mt Windsor Subprovince, Australia. Cambro-Ordovician. Reward: 1.2 Mt@ 5.5% Cu, 6.5 g/t Ag, 1.2 g/t Au. Highway: 0.2 Mt @ 3.5% Cu, 13 g/t Ag, 1 g/t Au.	Greenschist facies metamorphism.	Pipe-like py and cpy-py bodies cross-cutting local stratigraphy, minor stratiform lenses and stringers above and below ore bodies; largest body: 100 x 150 m in plan and up to 250 m thick.	Py-qtz stringer veins.	Submarine sandstone, siltstone and pumice breccia with syn-sedimentary rhyolitic, rhyodacitic and dacitic sills and domes, abundant peperite; MS in intrusive bodies. Enveloped by alteration pipe to at least 150 m below and up to 60 m above ore bodies: central qtz-ser-py, zone of ch-anh-gyp, ch-ser-qtz, outer zone of ch+ser.	Py-qtz stringer veins.	2 ore bodies-Highway & Reward; py-cpy lenses and pipes are enveloped by py-sph-cpy-ga-bar ore.	Py, cpy cores with outer edges containing sph, py, cpy bo and cov; minor ten; aikinite.	Ms enclosed in intrusive or mass-flow units; discordant and stratabound ores contain relics of precursor volcanic particles; peperite and ms are discordant to bedding. Replacement fronts pass from the pipes into the HW. HT alteration and veining extend into the HW without changes in intensity.	Sedimentary rocks became indurated by intrusion of syn-sedimentary felsic sills. Changes in permeability and porosity led to the focussing of fluids, which caused the pipe-like sub-seafloor deposition of the ore body by replacement.	Doyle & Huston 1999.
West Thalanga, Mt Windsor Subprovince, NE Australia. Cambro-Ordovician. Total Thalanga: 4.7 Mt@ 8.4 % Zn, 1.8% Cu, 2.6 % Pb, 69 g/t Ag, 0.4 g/t Au.	Upper greenschist facies metamorphism with strong D1 and D2 overprint.	One lens 300 m long and between 1-20 m thick. Stratabound.	Strongly altered volcanic and volcaniclastic rhyolite. Alteration zones include three types: A1-least altered qtz+feld+bio+ser, A2-moderately altered qtz+ser+ch+py+phlog., A3-stringer zone qtz+py+ser+ch.	Volcaniclastic sandstone and breccia with carb+trem+chl rocks and ms lenses. Distal part of ms zones have bar-sulfide and mgt+qtz+bar rocks.	Weakly altered dacite. Alteration may be unrelated to HT system associated with VHMS deposition.	Massive to semi-massive ore forming 2 associations within the lens (see morphology). Also patches within FW.	Massive pyrite with some cpy lens at base overlying FW, Carb++trem+ch encloses massive to semi-massive sp+ga+py +cpy.	Stratabound ms. Hosted by permeable volcaniclastic rocks where seawater and HT fluids mixed. Carbonate textures suggest space filling or uninhibited mineral growth in pore spaces. No exhalites.	HT fluid encountered seawater in permeable rocks close to the seafloor. This interaction deposited carbonate minerals and metals as HT fluid temperatures increased.	Hill 1996, Paulick & McPhie 1999, Herrmann & Hill 2001.

Table 7.4 cont.

Deposit Location. Age. Tonnage.	Deformation and Metamorphism.	Morphology.	Rocks and Alteration style.			Ore bodies.	Ore minerals.	Sub-seafloor characteristics.	Genesis.	References.
			Footwall.	**Host.**	**Hanging wall.**					
Currawong, Benambra Victoria, SE Australia. Silurian. 9.5 Mt @ 4.33% Zn, 1.65% Cu, 0.86 % Pb, 38g/t Ag, 1.3 g/t Au.	Strong deformation overprinting, but low metamorphic grade (lower greenschist). Early D1 foliation restricted to sedimentary rocks, intense D2 associated with foliations and folding. All dissected by D3 related to a major shear zone.	2 stratiform lenses, faulted into 5 pod-like ore bodies. The edges of the lenses are interfingered with the host sequence. Largest ore body is 225 m long by 40 m thick (from cross-section).	Turbidites, andesitic, dacitic and rhyolitic breccia and coherent units. Qtz+ser+cb(±ch+ep), qtz+ch, ch, sil., stilp+cb(±ch+tl+ep)assoc. with different mineralising stages. See genesis.	See Footwall.	HW of the upper lens consists of turbidites. See Footwall.	Two lenses are 50 m apart. No discordant stockwork, but a stringer zone occurs as the level of flat tabular sheets, extending only 5 m into the FW. Overall broad zonation from FW to HW with gradational boundaries between ore bodies: Pb-Zn ores grade into pyrite-Zn ores which in turn grade into massive pyrite ores. Reverse sequence into HW. Py-mgt in FW.	Pb-Zn ores: gal+sph+py+min or cpy and rare as-py. Pyrite ores: py+sph+cpy. Pyrite-magnetite ores: veins and stringers of sph+stilp+mgt+po+cpy in massive py. Stringer ores: sph,cpy, bi+el.	Overprinting of clastic rocks by alteration. Alteration fronts: pyrite in sandstone and selective alteration of more permeable laminae in turbidites and breccias. Edges of ore bodies display replacement fronts between ores and host stratigraphy. Relationships indicate that the sulfide-rich ores were produced by almost complete replacement of the host rock by sulfide. Lateral discontinuity and cyclicity in metal zonation is more akin to sub-seafloor replacement than exhalation models.	Three stages of formation: I. py+qtz+ser+cb±ch with Pb-Zn & py-Zn ores. II. Qtz+ch, massive banded pyrite. III. Py+qtz+cb, remobilising (?) interstitial py in massive & banded py. IV. Cpy veinlets assoc. with texturally destructive ch & qtz+ch. V. Bi-el veins. VI. sph+stilp veins assoc. py+mgt & sph stringers.	Bodon & Valenta 1995.

Alteration mineral abbreviations: ab=albite, and=andalusite, bar=barite, bio=biotite, cal=calcite, cb= carbonate, ch=chlorite, dol=dolomite, ep=epidote, feld=feldspar, ga=garnet, gah=gahnite, gyp=gypsum, hb=hornblende, kyan=kyanite, mic=microcline, plag=plagioclase, qtz=quartz, ser=sericite, sid=siderite, sil=silica, stilp=stilpnomelane, t=talc, tm=tourmaline, trem=tremolite.
Ore mineral abbreviations: Ag-py=argenopyrite, as=aresenopyrite, bi=bismuthanite, bo=bornite, cas= cassiterite, cov=covellite, cpy=chalcopyrite, el=electrum, ga=galena, mgt=magnetite, po=pyrrhotite, sph=sphalerite, st=stannite, ten=tennatite, tet=tetrahedrite
Other abbreviations: , FW=footwall, HT=hydrothermal, HW=hanging wall, ms=massive sulfide.

sediments (Chapter 8) and many fine-grained siliciclastic sediments were silicified (Stage 1, Fig. 7.18).

The highest concentrations of massive sulfide are within the upper carbonate lens, although the lower carbonate lens in the central portion of the prospect has not been adequately tested. The most likely cause for sulfide deposition is increasing pH, which may or may not be accompanied by cooling (Large 1977). An acidic, metal-bearing fluid is normal for many VHMS-forming hydrothermal fluids, e.g., pH 4.2–4.7 for Kuroko deposits (Pisutha-Arnond & Ohmoto 1983), pH 3.2 of fluids venting from the Juan de Fuca Ridge (von Damm 1990) and pH 2.5–4 for fluids from many modern black smokers (Seyfried et al. 1999). If such a fluid encountered the carbonate lenses at Onedin, dolomite would have been dissolved, thereby increasing the pH of the fluid. A pH shift of only 1 unit at 250°C could deposit much of the Zn, Cu and Pb carried by a hydrothermal fluid at close to saturation/super-saturation levels (Solomon & Walshe 1979, Cooke et al. 2000; Stage 2, Fig. 7.18). More abundant pyrite at the edges of the carbonate lens could have formed either (1) as the ore-forming fluid cooled at the outer margins of the carbonate, (2) from increased fluid pH, which would also deposit more chlorite, or (3) conversion of precursor pyrrhotite or monosulfide by oxidation near magnetite-rich sediments. Any one, or combination of these processes may have contributed to the deposition of pyrite at the margins of the upper carbonate lens. Another possibility, which cannot be discounted, is that the pyrite grew from pyrrhotite during deformation.

Chlorite schist-hosted sulfide mineral accumulations sit above or between the carbonate lenses. These deposits were probably formed from evolved hydrothermal fluids, which had passed through the carbonate lens. After the hydrothermal fluid had reacted with carbonate and deposited sulfide minerals, it would have an increased pH and pCO_2, depleted H_2S and lower metal abundances compared to the original fluid. The evolved hydrothermal fluid would retain some chalcophile elements in solution if all H_2S was exhausted before all the metals were deposited. The pore waters and open spaces in the sub-seafloor environment, which contained carbonaceous material in black mudstone, probably also contained H_2S. Mixing the evolved hydrothermal fluid with the pore waters would result in a drop in fO_2 of the ore fluid and replenishment of H_2S, precipitating the chalcophile elements in sulfide minerals such as sphalerite, galena, chalcopyrite and pyrite. Carbonate minerals would precipitate as pCO_2 in the evolved fluid was reduced (Stage 3, Fig. 7.18).

Carbonate, talc and Mg-rich chlorite are the main gangue minerals in the massive sulfide deposits at Onedin. These minerals reflect high Mg in the hydrothermal fluid, probably originally derived from seawater and/or the breakdown of Mg-rich minerals. All were probably deposited in association with the sulfide minerals as the pH of the fluids increased (Large 1977). Fe-rich dolomite is often associated with the sulfide minerals and probably reflects deposition from the hydrothermal fluid which has incorporated carbonate and reached higher pH (Fig. 7.19). The sequence of gangue minerals in the chlorite schist–hosted sulfide reflects a decrease in temperature and pH as many veins and deposits have a chlorite-rich outer edge grading into abundant talc, carbonate and quartz associated with the sulfide minerals internally (Fig. 7.19).

The lack of paragenetic constraints on the sulfide minerals means that they may have formed at different times, from different fluids. It is conceivable that an early hydrothermal alteration zone

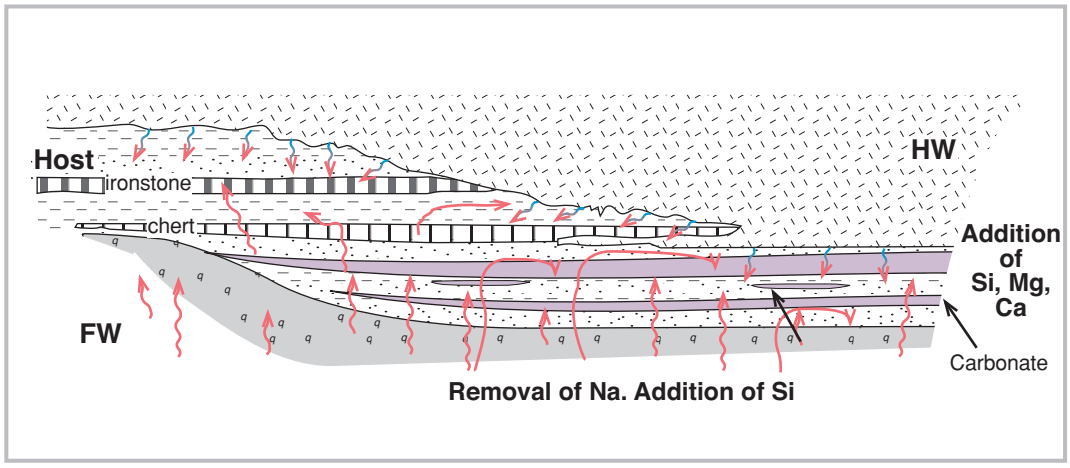

Stage 1: Sub-seafloor fluid circulation in response to rise in T. Fluids circulate in porous volcaniclastic units and through sediments. Rhyolite and enclosing indurated sediments form a cap to fluid movement. The low T fluids penetrate along porous vitriclastic and calcareous mud(?) to deposit carbonate. Silica is deposited in siliceous fine sand and mud (Chapter 8).

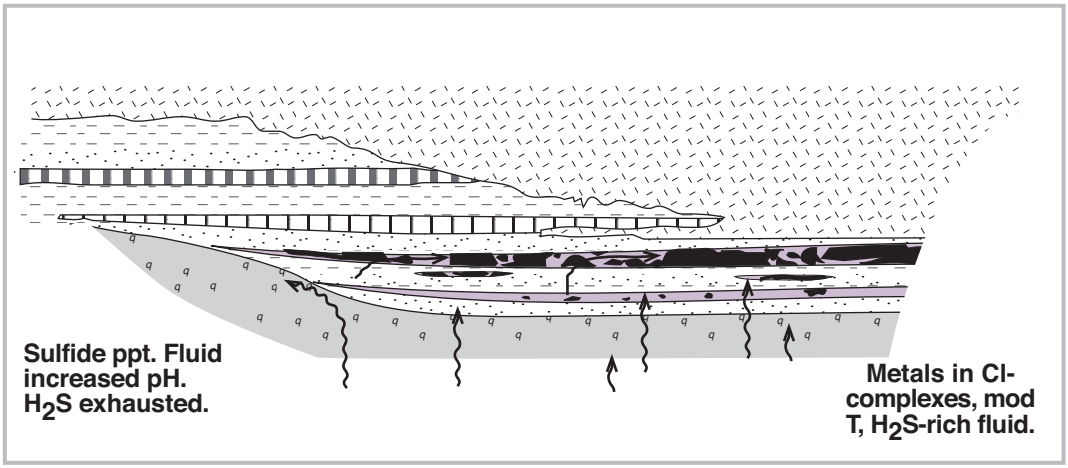

Stage 2: Metal-bearing fluid (seawater salinity, acid, T around 200º-300º C, metals in chloride complexes, H_2S-rich) encounters the carbonate alteration below the seafloor. Replacement of carbonate by the acid fluid causes deposition of Zn, Pb, Fe and Cu sulfide minerals. Minerals precipitated include sphalerite, some galena, pyrrhotite, less abundant pyrite and chalcopyrite, accessory silver sulfosalts.

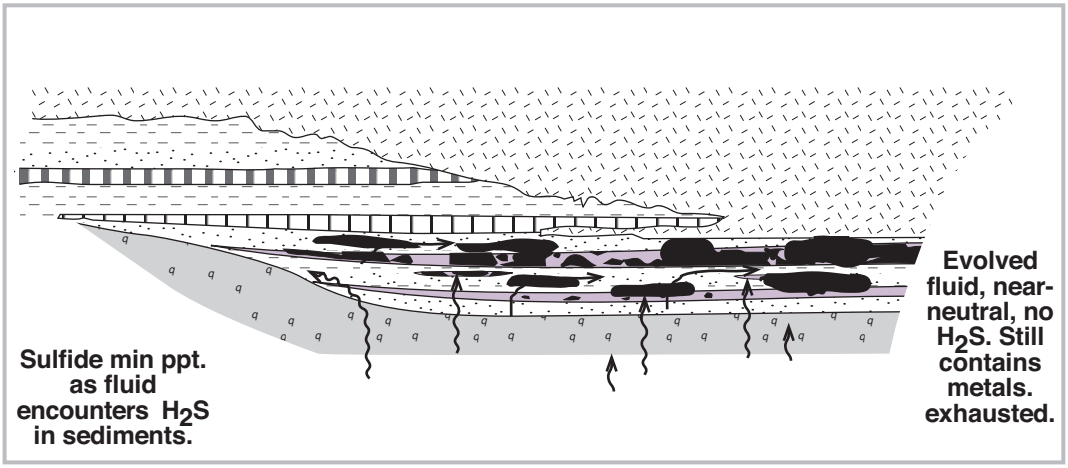

Stage 3: Evolved hydrothermal fluid (seawater salinites, near-neutral(?), T around 200º-300ºC, metals in chloride complexes, H_2S-depleted) encounters the pore water in the sediments below the seafloor. The carbonaceous sediments contain H_2S which triggers deposition of Zn, Pb, Fe and Cu sulfide minerals. Minerals precipitated include sphalerite, some galena, pyrite, chalcopyrite and less abundant pyrrhotite.

Figure 7.18 Genesis model for base metals at Onedin.

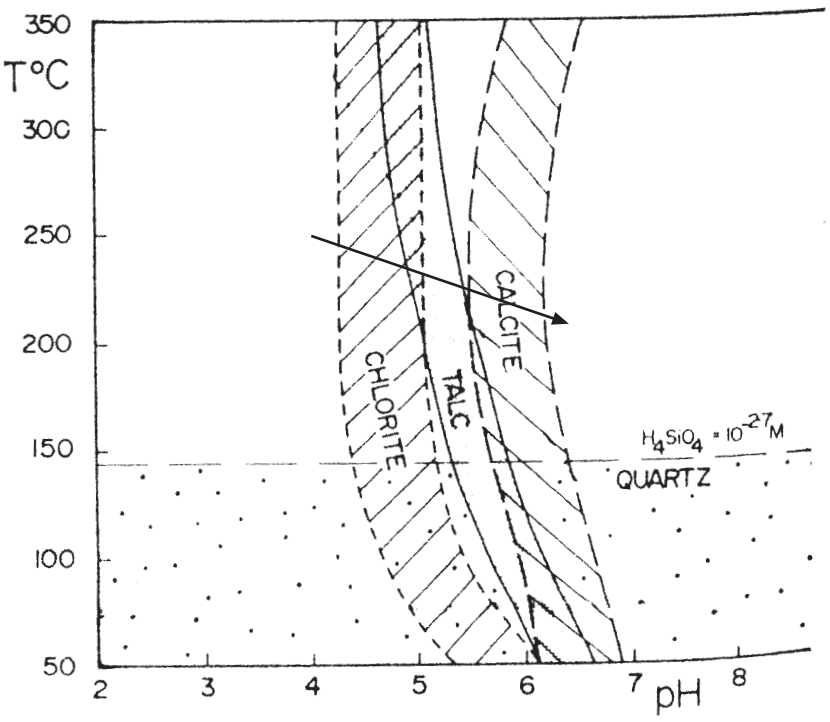

Figure 7.19 Temperature-pH stability fields for some of the gangue minerals common at Onedin (Large 1977 from data of Helgeson 1969). Higher Fe-abundance shifts the mineral stabilty fields left to lower pH. Deposition of chlorite, talc and carbonate associated with the sulfide minerals at Onedin can all be deposited from an acidic hydrothermal fluid as it reacts with carbonate and increases pH. A possible path is arrowed.

was overprinted by later, low- to moderate-temperature, pre-metamorphic fluids causing carbonate replacement. The main sphalerite carbonate replacement with some galena may have deposited from early low temperature fluids, consistent with correlation in the metal abundances of Pb, Zn and Ag. Subsequent, hotter fluids may have overprinted these sulfide minerals and deposited iron and copper sulfide minerals. Nevertheless, the model outlined above (Fig. 7.18), provides the simplest explanation for the base metal occurrence at Onedin. It encompasses mineralisation and alteration into a related series of events with evolving fluids and co-precipitation of all the sulfide minerals.

7.9 CONCLUSION

At Onedin, few early hydrothermal minerals survived metamorphism, many features are deformation-related and the sulfide zones were annealed and remobilised. However, geochemistry of the alteration halo is consistent with alteration patterns at VHMS deposits. Low Na abundances characterise the footwall and host sequence and Mg, Ca and Si are abundant in the minerals of the host sequence. This alteration pattern is the most compelling evidence for a VHMS origin for sulfide mineralisation at Onedin. Overprinting of the hanging wall sill by alteration indicates a sub-seafloor hydrothermal system.

Metal abundances classify the Onedin deposit as a Zn-Cu deposit with abundant Zn-Cu-Pb portions. No distinct copper or zinc rich zones were recognised. Zinc ratios (ZR=100 Zn/Zn+Pb)

are high (83.3), but rather than being Pb-poor, comparison with other deposits suggest that Onedin is better viewed as a zinc-rich deposit.

Comparison with modern and ancient sub-seafloor VHMs deposits suggests that the replacement style of the chlorite schist-hosted ore in sedimentary sequences is well documented, e.g., Middle Valley, Currawong and Ansil. However, the carbonate-replacement style of the high grade massive sulfide at Onedin has no modern analogue and is uncommon in ancient VHMS deposits.

A simple model for the base metal mineralisation at Onedin is as a sub-seafloor VHMS deposit. Early low temperature fluid circulation developed carbonate and silica alteration. As circulation intensified, an acidic, H_2S-bearing, hydrothermal fluid with the metals in chloride complexes produced the replacement sulfide minerals and massive sulfide deposits in the carbonate lenses. This fluid dissolved carbonate, and deposited sulfide minerals until the sulfur source was depleted. Evolved fluid moving out of the carbonate would have increased pH and pCO_2. As the evolved, cooling fluid interacted with pore waters in the surrounding carbonaceous sediments and fractures, pCO_2 decrease caused deposition of carbonate and the H_2S in the pore waters allowed the deposition of the remaining metals.